targets

MDPI

Review

Systematic Reversal of Drug Resistance in Cancer

Shujie Zhu, Xuemei Wang * and Hui Jiang *

State Key Laboratory of Digital Medical Engineering, Jiangsu Key Laboratory for Biomaterials and Devices, School of Biological Science and Medical Engineering, Southeast University, Nanjing 210096, China; zzshujie@163.com

* Correspondence: xuewang@seu.edu.cn (X.W.); sungi@seu.edu.cn (H.J.)

Abstract: Drug resistance in cancer is a significant contributor to high mortality, and it exists in the complex form of a multi-parameter. Here, we unravel the roles of tumor heterogeneity, intratumoral physiological barriers, and safe havens in the onset and progression of cancer drug resistance, and outline strategies for resolution. We advocate for a "three-step approach" to reverse cancer drug resistance, including the management of cancer evolution and early intervention, the normalization of intratumoral physiological barriers, and the breakage of tumor safe havens. This approach aims to effectively manage the source of drug resistance, dismantle the breeding grounds of drug resistance, and break the sanctuaries where drug resistance hides.

Keywords: cancer; drug resistance; tumor heterogeneity; physiological barrier; blood–brain tumor barrier

1. Introduction

Until now, cancer has remained as one of the diseases with the highest incidence and mortality rates worldwide. In 2020, a global report documented 19.3 million cases of cancer, resulting in 10 million deaths [1]. A survey conducted by multinational pharmaceutical companies in 2023 revealed that global spending on anticancer drugs reached approximately USD 218 billion that year, with projections estimating a rise to USD 375 billion by 2027. Despite this substantial investment in cancer treatment, the cure rate and patient survival rates continue to fall short of expectations. Drug resistance in cancer stands out as a significant factor contributing to this issue.

Since the development of nitrogen mustard hydrochloride in the 1940s, chemotherapeutic agents have undergone gradual advancement. To date, over 50 chemotherapy drugs targeting various types of tumors have received approval for marketing, which include alkylating agents (e.g., cyclophosphamide), antimetabolites (e.g., fluorouracil and methotrexate), anti-tumor antibiotics (e.g., pingyangmycin and bleomycin), anti-tumor natural products (e.g., vinblastine and paclitaxel), hormonal agents (e.g., medroxyprogesterone and prednisone), and miscellaneous agents (e.g., platinum compounds). Despite achieving satisfactory anti-tumor effects initially, these drugs may lose their efficacy over time due to the development of drug resistance, ultimately resulting in disease recurrence.

Initially, the primary approach to combating single-drug resistance involved employing multi-drug combinations. While these combinations effectively delay the onset of drug resistance, they also contribute to the emergence of more complex forms of tumor resistance, including multi-drug resistance (MDR) and the proliferation of various tumor subclones. It means tumor cells exhibit resistance to multiple drugs, with characteristics of cross-resistance and non-specific resistance. As drug resistance gradually increases, even with clinical adjustments in drug order and use, the tumor can continue to grow or recur. Traditional treatments like surgery, chemotherapy, and radiotherapy are no longer adequate to meet the current demands of cancer treatment. Therefore, it is crucial to identify the sources and mechanisms of tumor drug resistance in order to effectively control its development.

check for updates

Citation: Zhu, S.; Wang, X.; Jiang, H. Systematic Reversal of Drug Resistance in Cancer. *Targets* **2024**, 2, 250–286. https://doi.org/10.3390/targets2030015

Academic Editor: Bruno Rizzuti

Received: 30 May 2024
Revised: 25 July 2024
Accepted: 2 September 2024
Published: 13 September 2024

Here, we have constructed a foundational framework for understanding drug resistance in tumors, delineating its primary causes and its ramifications for tumor treatment. We advocate for a "three-step approach" to reverse cancer drug resistance, including the management of cancer evolution and early intervention, the normalization of intratumoral physiological barriers and the breakage of tumor safe havens. This approach aims to effectively manage the source of drug resistance, dismantle the breeding grounds of drug resistance, and break the sanctuaries where drug resistance hides.

2. Ecology and Evolution of Drug Resistance

Before challenging tumor drug resistance, it is crucial to thoroughly understand its source, breeding grounds, and havens. This entails comprehending the heterogeneity caused by gene mutations that trigger drug resistance, collapsed blood–lymph networks and excessive matrix hardening which result in inadequate perfusion, and the blood–brain barrier/blood–brain tumor barrier which provides a safe haven for tumors, thereby comprehensively assessing the factors driving the emergence and progression of drug resistance (Figure 1).

2.1. The Source of Drug Resistance: Tumor Heterogeneity

Tumor heterogeneity means that tumors divide and proliferate multiple times during the growth process, showing changes in molecular biology or genes, resulting in differences in growth rates, invasion ability, drug sensitivity, prognosis, and other aspects. These processes range from frequent gene editing by enzymes of the family apolipoprotein B mRNA-editing enzyme catalytic polypeptide-like (APOBEC) cytidine deaminases to large-scale chromosomal changes, leading to loss of genomic material and triggering macroevolution [2,3] both of which gradually promote the development of tumor drug resistance. In 1958, evolutionary biologist Julian Huxley commented that "the occurrence and development of new mutations in the genetic heterogeneity of cancer are very interesting". However, it was not until sequencing technology gradually matured that the spatial and temporal genomic diversity of tumor heterogeneity was formally revealed. Studies have shown that 0 to 8 million coding mutations are found heterogeneously within primary tumors, within metastatic tumors, and at sites of tumor recurrence [4,5].

Primary heterogeneity during tumorigenesis leads to natural resistance to certain types of drugs, which is called primary resistance. Clinically, non-responders are those who show no tumor shrinkage after starting treatment. For example, colorectal cancer cells show high resistance to basic chemotherapy agents at the beginning of treatment. Mutations in multiple genes (e.g., CRBN, CUL4B, NR3C1, RARA, and CD38) in refractory multiple myeloma make it primary drug-resistant to immunomodulatory imide drugs, synthetic glucocorticoids, and monoclonal antibodies [6]. Primary drug resistance is mostly related to missense mutations and truncating mutations (frameshift, stop-gain, and splice site) in drug binding-related genes. The mutations prevent the drug from binding to the target protein pocket, thereby producing drug resistance [7,8].

In addition, during the development of tumors, the resistance that develops in response to treatment pressure is called acquired resistance. The development of tumor heterogeneity driven by therapeutic pressure has been well characterized in previous studies, ranging from the disappearance of targeted cellular clones to the acquisition of new drug-resistant mutations and to adaptive responses in signaling and epigenetics, which causes the end result of a complete change in tumor phenotype [9,10]. In fact, clonal burden and subclonal mutation burden are not completely equal during tumor development. For example, in the case of low-grade glioma treated with temozolomide, the pressure of treatment can cause it to relapse and transform into a highly aggressive glioblastoma. In cases where the clonal burden is significantly lower than the subclonal mutation burden, a large number of subclonal mutations are directly related to therapeutic agent-induced resistance mutations. At the same time, the lack of a mismatch repair mechanism may further exacerbate the burden of subclonal mutations [5,11]. Not singly but in pairs, research on clonal

hematopoiesis (CH), a recurrent somatic mutation in leukemia-associated genes, found that the most commonly related mutated genes PPM1D and TP53 were associated with previous chemotherapy exposure received by patients ($p = 0.047$ and $p < 0.001$, respectively). CH-related mutations lead to an increased incidence of subsequent hematological tumors and myelodysplastic syndromes (MDS), as well as resistance to basic chemotherapy, promoting the development of related drug-resistant mutations [12,13]. The parallel development of similar events prompts us to carefully weigh the adverse consequences of treatments and to conduct more in-depth prospective longitudinal studies on the mechanisms driving tumor "evolution of drug resistance" and "drug-resistant recurrence and metastasis".

2.2. The Breeding Grounds of Drug Resistance: The Intratumoral Physiological Barrier

The tumor microenvironment may mediate drug resistance through multiple mechanisms, including impeding drug delivery efficiency and preventing immune clearance. Although research on nanotechnology in recent years has found that enhanced permeability and retention effects are the mainstays of nanoparticle treatment of solid tumors, it cannot deliver these particles uniformly and in sufficient amounts to all areas of the tumor. This heterogeneous distribution of drugs is primarily the result of physiological disturbances caused by abnormal "hemato-lymphatic networks and extracellular matrix" in the tumor microenvironment.

2.2.1. Blood–Lymph Network

Most anticancer drugs are transported through the blood, and blood vessel morphology and blood flow velocity directly affect the movement of drugs in the blood vessels. Within the tumor, the hierarchical structure of blood vessel branches is unclear, the spatial distribution is uneven, and the shape is tortuous [14]. Compared with the blood vessels of normal tissue, the shape, structure, and distribution of tumor blood vessels are extremely irregular, which directly affects the efficiency of drug delivery within the tumor [15]. The structure of tumor blood vessel walls is abnormal, and endothelial cells are often poorly connected or overlapping [16], while the basement membrane is abnormally thick or thin, and there are palisades and transendothelial channels with pores of hundreds of nanometers. The irregular structure of the blood vessel wall causes uneven permeability and finally collapses due to solid stress generated by tumor proliferation or metastasis [17,18]. In addition, according to the perfusion rate, the tumor can be divided into the avascular necrosis region, the semi-necrosis region, the stable microcirculation region, and an advancing front of uneven size [19]. The existence of regions without vascular necrosis puts tumors in a harsh environment of low oxygen partial pressure and low pH value, which promotes the tumor's invasiveness to expand the advancing front. Several conventional therapeutic drugs, such as doxorubicin and methotrexate, require oxygen to exert their tumor-killing effects, so the activity of these drugs is significantly reduced in poorly perfused, hypoxic areas [20]. This uneven perfusion also makes it difficult for hyperthermia drugs to heat around the tumor [21,22]. Compared with non-perfused regions of tumors, vascular permeability and hydraulic conductivity in perfused regions are usually significantly higher than in normal tissue [17], so these vessels may lack permeability selectivity [23,24].

Similar to the above-mentioned vascular collapse, in the early stages of tumor development, lymphatic vessels will also be compressed by the solid stress of tumor proliferation and lose their function [25]. Even though reducing the pressure exerted by the proliferating cell mass can restore the tissue morphology of the lymphatic vessels, it does not restore their function. Obstacles to intratumoral lymphatic vessels, whether due to compression of the tissue structure, an impaired lymphatic clearance function, or blocked blood vessels by metastatic cancer cells, lead to an increase in intratumoral interstitial fluid pressure, thereby hindering drug delivery to the tumor [26]. Subsequently, due to the destruction of the lymphatic vessel structure and increased permeability, cancer cells invade lymphatic vessels, promoting cancer metastasis.

The high permeability of tumor blood vessels and the loss of functional lymphatic vessels cause intratumoral interstitial high pressure. There is a steep pressure gradient

from the center of the tumor to the edge of the tumor, and the edge pressure is close to that of normal tissue [27–29]. Interstitial high-pressure results in less transvascular convective transport of macromolecular drugs in the tumor center than in the tumor periphery [28,30], and as the tumor weight increases, transvascular exchange will also be reduced due to the decrease in the average vascular surface area per unit of tissue weight [31]. At the same time, because the interstitial fluid pressure in the center of the tumor is higher than that of the surrounding tissue, the interstitial fluid will move from the periphery of the tumor to the surrounding normal tissue, and 14% of the plasma entering the tumor also leaves from the periphery of the tumor [17,32]. Therefore, drug macromolecules lingering on the periphery of the tumor must overcome this outward convection in order to diffuse into the tumor, which undoubtedly greatly reduces the delivery efficiency of drug macromolecules [18].

In short, with the abnormal increase in solid pressure distribution generated by tumor proliferation, the blood–lymph network gradually collapses, thereby promoting tumor progression, immunosuppression, inflammation, invasion, and metastasis, and reducing the efficacy of chemotherapy, radiation, and immunity [33,34].

2.2.2. Extracellular Matrix

The extracellular matrix (or matrix) is a ubiquitous non-cellular component in all tissues and organs of the body. It is usually secreted and assembled into insoluble entities. It plays an important role in the development of organisms, tissue repair, and the maintenance of tissue and organ homeostasis [35]. There is a complex relationship of "dynamic reciprocity" between matrix and cells. Cells deposit, decompose, and remodel the matrix, while the matrix affects cell proliferation, migration, invasion, and changes in tissue morphology [36]. This means that the matrix is the cornerstone of tissue and organ physiology. During tumor development, the matrix becomes highly dysregulated and is altered at the biochemical, biomechanical, and topographic levels.

With the development of biomedical engineering methods, hydrogels and scaffold materials with multiple structural and signaling components have been designed to more accurately simulate and reproduce the heterogeneity of the tumor microenvironment. A large number of studies have clarified the evolution and mechanism of the matrix during tumorigenesis [37,38], which also dictates the response to therapy. We have also begun to see the deployment of matrix-centric, matrix-targeting cancer therapies.

Clinical resistance to chemotherapy is often related to tumor stiffness. Studies have found that softer tumors (breast tumors) respond more sensitively to chemotherapy than harder tumors (fibroids). The biochemical and biomechanical properties of matrices are modulated by different components, concentrations, and assembly. These properties are further regulated in subsequent processes through post-translational modifications of matrix components through hydroxylation, glycosylation, sulfonation, cross-linking, cleavage, and degradation [39].

The main matrix components that control tumor stiffness are collagen (fibrillar collagen types I and IV), glycoproteins, and proteoglycans. Fibrous collagen type I is the main component of tumor connective tissue and is highly aligned and anisotropic in tumors (isotropically oriented in healthy tissue) [40,41]. Type IV collagen is mostly distributed in the basement membrane, which together with laminin, defines discrete boundaries beyond which tumor invasion and metastasis need to break. Glycoproteins and proteoglycans, on the other hand, fill the interstitial space and buffer the physical stress on the matrix due to their high viscosity generated by their side chains and their ability to resist compressive forces. At the same time, by regulating cellular processes and matrix molecular assembly, it combines "growth factors, cytokines and divalent cations" to build a more cohesive matrix molecular network [42], and exhibits the effect of promoting the development of drug resistance in most solid tumors.

Post-translational modifications of the matrix are controlled by several intracellular and extracellular enzyme families, and dysregulation of any one or more enzyme families may lead to changes in matrix stiffness (matrix deposition and remodeling) which is

associated with cancer drug resistance [43]. In addition, excessive matrix cross-linking is common in most desmoplastic tumors. Excessive cross-linking of the matrix leads to the accumulation of a dense network of matrix molecules, a reduction in matrix turnover, and an increase in the longevity of protumorigenic matrix molecules in the extracellular space [44,45].

During the progression of most solid tumors (including but not limited to breast cancer [46], ovarian cancer [37], and pancreatic cancer [47,48]), the abundance of extracellular matrix molecules (collagen, glycoproteins, proteoglycans, hyaline, hypoglycemia, laminin, and fibronectin) is increased and accumulates in the stroma to form desmoplastic tumors; matrix molecules are excessively cross-linked into a dense network, leading to matrix hardening and altered mechanosensory pathways, promoting tumors drug resistance [49,50]. Integrin heterodimers are major links in cell–matrix communication and are associated with the activation of numerous downstream signaling networks. When the matrix hardens, integrins (such as $\alpha_5\beta_1$, $\alpha_v\beta_3$, $\alpha_v\beta_5$, $\alpha_v\beta_6$, and $\alpha_6\beta_4$) mediate the formation of connective tissue and activate the drug resistance cascade of tumor growth and invasion by binding to relevant ligands [51]. Studies have found that if the $\alpha_5\beta_1$ integrin is overexpressed in pancreatic cancer, cancer-associated fibroblasts (CAFs) are activated, tumor proliferation increases, and tumor perfusion decreases, thereby reducing the efficacy of gemcitabine in in vivo models [48]. Increased laminin deposition in breast tumors can also activate the $\alpha_6\beta_4$ integrin and increase signaling through the transmembrane proteins CD151 and FAK, leading to resistance to trastuzumab [52]. Clinically, treatment-induced increases in fibrin abundance have also been associated with doxorubicin resistance in breast cancer [53]. In addition, drug resistance can also be achieved through matrix remodeling that activates downstream signaling, such as melanoma cell-associated fibroblasts inducing matrix remodeling, promoting integrin β1-FAK-Src signaling, activating ERK signaling, and causing BRAF inhibition resistance [54]. Similarly, research in the field of anti-angiogenic therapies has shown that the matrix is resistant to treatment through the release of PDGF-C from CAFs [55]. Taken together, these examples suggest how excessive matrix "deposition, aggregation, cross-linking, and remodeling" and changes in matrix component abundance that stimulate downstream channel activation reduce the efficacy of anti-tumor drugs and promote the development of drug resistance.

2.3. The Safe Havens of Drug Resistance: The Blood–Brain Barrier/Blood–Brain Tumor Barrier

In addition to tumor heterogeneity and extracellular matrix barriers, the existence of "safe harbor" sites in the human body provides effective shelter for tumor colonization and proliferation, which are anatomical spaces where systemic drugs cannot reach therapeutically effective concentrations. The most typical example is the blood–brain barrier (BBB), which serves as a protective barrier for the central nervous system (CNS).

The BBB tightly regulates CNS homeostasis through the neurovascular unit, including endothelial cells, pericytes, and astrocyte endfeet. The BBB allows the influx of circulating molecules relevant to the regulation of CNS function and the efflux of toxic cellular byproducts, and prevents the effective entry of foreign drug molecules [56]. In a non-diseased brain, protective barriers involve transport barriers, enzymatic barriers, and immune barriers, with transport barriers being dominant [57]. The transport barrier function is primarily supported by tight junctions (regulating the paracellular transport) and active efflux transporters (AETs). Tight junctions control the passage of large and small molecules through paracellular transport (biological compounds are restricted in diffusion, while hydrophobic small molecules are allowed to permeate) [58,59]; AETs (e.g., P-glycoprotein and breast cancer drug resistance protein) work through recognition, then actively pump out the antitumor drugs of the cells returned to the bloodstream for "detoxification", preventing the drugs from entering the CNS and reducing the amount of brain accumulation of anti-tumor drugs [60,61]. AETs control the entry of most anti-brain tumor drugs (approximately 70% of commercially available anticancer drugs), thereby strengthening the defensive nature of the tumor "safe haven" [62].

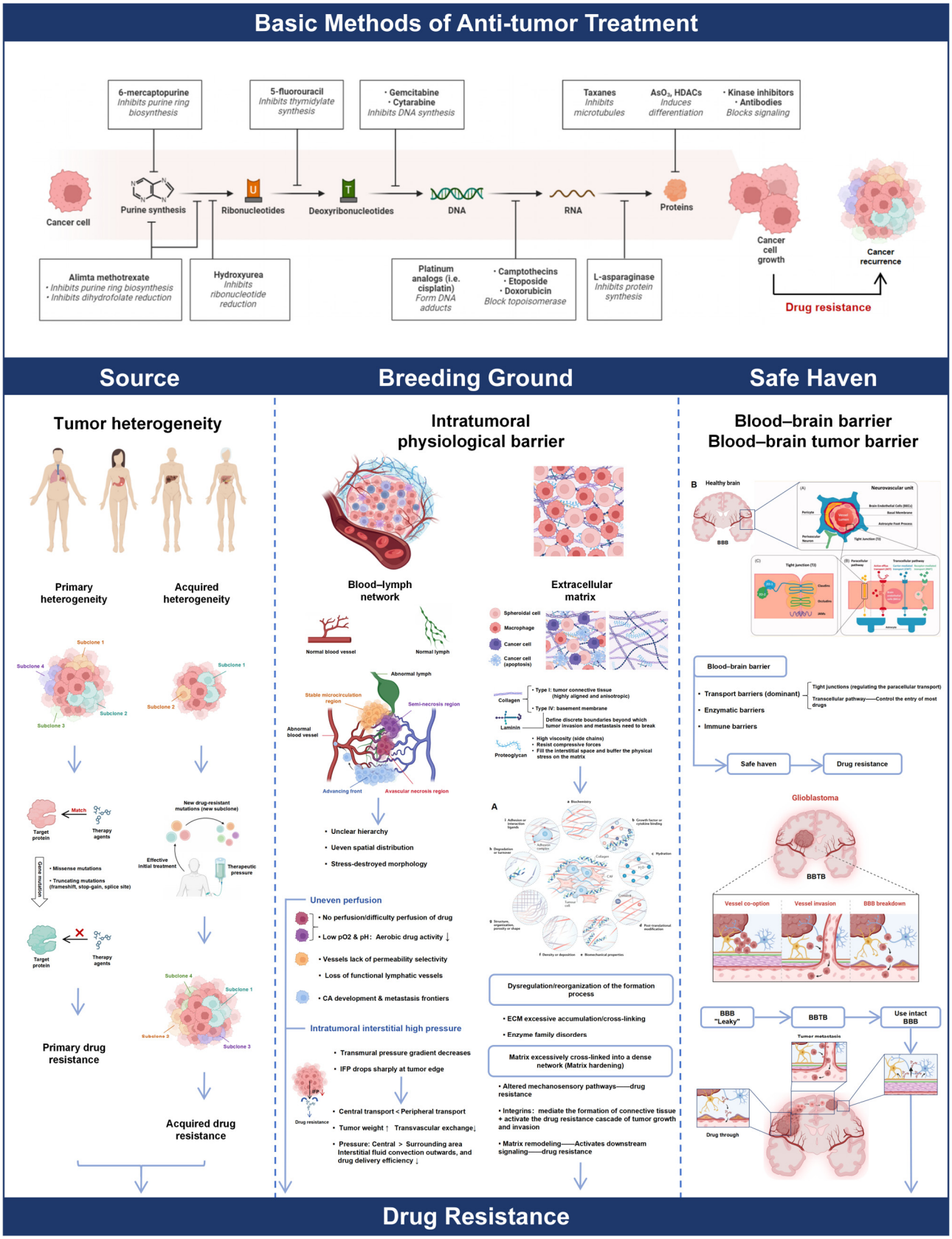

Figure 1. Drug resistance in cancer. (**A**) Matrix changes in cancer [39]; (**B**) schematic representation of (A) neurovascular unit; (B) paracellular transport pathway and transcellular transport pathway of BBB; (C) tight junction (TJ) associated components [62]. (Figure was created by biorender.com accessed on 30 August 2024).

When tumors are present, the integrity of the BBB is destroyed, forming a blood tumor vasculature. The matrix and cancer cells in the brain tumor microenvironment redefine the permeability of blood vessels and tumor proliferation and metastasis. Although the blood–brain tumor barrier has higher permeability, heterogeneous permeability and the perfusion rate of drug molecules lead to unsatisfactory drug delivery rates and accumulation rates, which also lead to the emergence of a tumor "safe harbor" [63–65]. Malignant glioma is the most lethal primary brain tumor. It is characterized by the overexpression of P-glycoprotein on endothelial cells and shows high activity at the intact BBB tumor border [66]. This suggests that even with a "leaky" blood–tumor barrier (BTB), highly invasive brain tumors can still extend into healthy brain parenchyma areas and utilize the intact BBB tumor boundary to inhibit chemotherapy agents from entering the brain [67], which may explain the minimal efficacy of most anticancer drugs in highly aggressive brain tumors [57,62].

In summary, the blood–brain barrier provides a "safe harbor" for tumors, hinders the entry of a variety of anti-tumor drugs, and poses a huge obstacle to the treatment of brain metastases and primary brain tumors.

3. Overcoming Drug Resistance

Tumor drug resistance, influenced by numerous factors, has evolved into a complex network of multi-parameter regulations, dependent on time and space. With advances in medicine and bioengineering, the "parameters" associated with drug resistance have been increasingly analyzed and studied. Consequently, treatment strategies targeting the onset and progression of anti-tumor drug resistance have been proposed. In the following sections, we delve into how a "three-step approach" can leverage vulnerabilities in tumor heterogeneity, the tumor microenvironment, and safe havens to address resistance at its source, eradicate the breeding grounds of resistance, and dismantle the sanctuaries of resistance.

3.1. Managing the Source of Drug Resistance

3.1.1. Management of Cancer Evolution and Early Intervention

The conventional approach to cancer management has predominantly focused on addressing acquired drug resistance. However, with the ongoing analysis of clonal and subclonal mutation patterns in cancer, there appears to be the potential to predict the future evolutionary trajectories of tumors and manage their primary drug resistance. Copy number and mutation data obtained from temporally and spatially distinct biopsies of various tumor types have become available. These datasets are then subjected to algorithmic analysis using bioinformatics tools, which segment subclonal copy number alterations and loss of heterozygosity, target the tumor phylogenetic tree, and utilize the inferred subclonal mutation incidence to construct a tumor subclonal hierarchy (Figure 2C) [68–71]. This process is crucial for uncovering the mutation patterns that drive tumor evolution and heterogeneity (Figure 2A,B) [9].

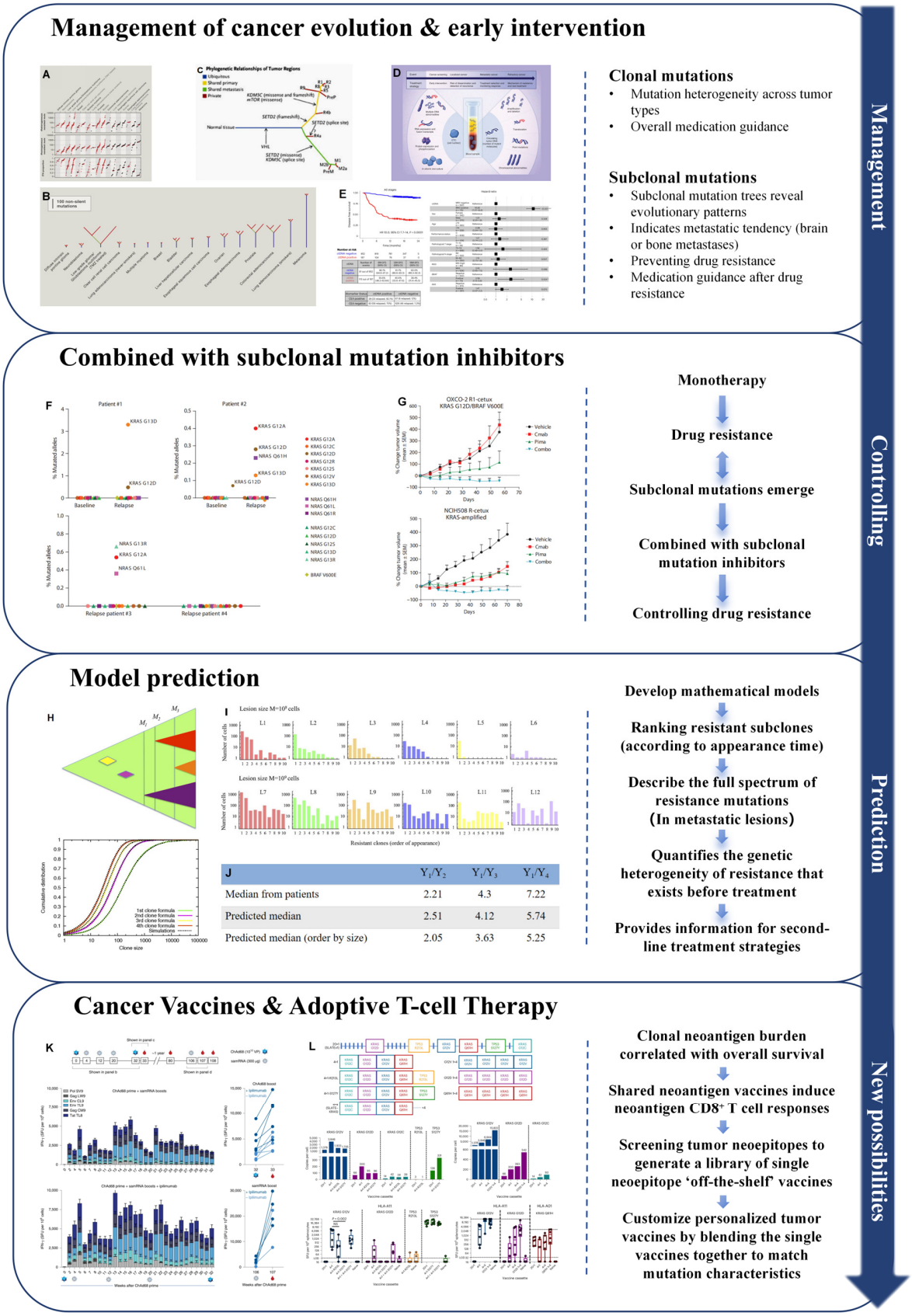

J	Y_1/Y_2	Y_1/Y_3	Y_1/Y_4
Median from patients	2.21	4.3	7.22
Predicted median	2.51	4.12	5.74
Predicted median (order by size)	2.05	3.63	5.25

Figure 2. Management of cancer evolution and early intervention. (**A**) The heterogeneity of non-silent mutations from multiple-sample sequencing across a range of cancer types (black circles represent treatment naive tumors, with red triangles indicating tumors that have received treatment) [9]; (**B**) evolutionary trees illustrating intratumor heterogeneity across cancer types [9]; (**C**) phylogenetic

relationships of the tumor regions [68]; (**D**) clinical applications of CTC and ctDNA analyses in cancer care [72]. (**E**) ctDNA-based MRD testing is predictive of survival outcomes in postsurgical patients with colorectal cancer [73]. (**F**) A BEAMing analysis of circulating tumor DNA of patients with acquired resistance to cetuximab or panitumumab displays complex patterns of KRAS and NRAS mutations [74]. (**G**) Resistance to EGFR therapy is reversed by pharmacological inhibition of EGFR and MEK (a combinatorial treatment with cetuximab plus pimasertib is effective in inducing tumor shrinkage in vivo) [74]. (**H**) The evolution of resistance in a metastatic lesion. As the lesion (green) grows from one cell to a detectable size, new resistant subclones appear. Some of them are lost to stochastic drift (yellow and pink), while others survive (purple, red and orange triangles). Instead of looking at the time of appearance of new clones, the approach takes into account the total size of the lesion when the resistance mutation first occurred [75]. (**I**) Resistant subclones in metastatic lesions [75]. (**J**) The number of circulating tumor DNA (ctDNA) fragments per milliliter (Y1 to Y4) harboring different mutations associated with resistance to anti-EGFR agents in colorectal cancer patients treated with an EGFR blockade. The ratio of resistant clone sizes is given by the ratio of the ctDNA counts for any two resistance-associated mutations [75]. (**K**) Heterologous vaccination with ChAd68 and samRNA induces broad, durable $CD8^+$ T cell responses in NHPs that are detectable long-term and can be boosted $\geq$ 2 years after their prime [76]. (**L**) The removal of immunodominant epitopes and repetition of epitopes leads to increased target density and T cell response to KRAS mutant neoantigens [77].

The analysis of clonal mutation data can identify genes with identical or similar tumor mutations and offer guidance for targeted drug therapy (Table 1). Subclonal mutations can indicate the likelihood and direction of tumor metastasis, such as bone and brain metastases, and also contribute to drug resistance [78]. In clinical practice, blood-based testing technologies utilizing circulating tumor DNA (ctDNA) and circulating free DNA (cfDNA), and continuously monitor the progression of these mutations within tumors [79]. Leveraging these highly sensitive and wide dynamic range technologies, researchers have delineated the subclonal mutation mechanisms responsible for acquired resistance to some specific targeted therapies in solid tumors (Table 2). Subclonal mutations typically confer drug resistance through several mechanisms: 1. The overexpression (amplification) of drug targets (receptor kinases) [80,81]. 2. The activation of downstream pathways or alternative bypass pathways related to the target [82–85]. 3. Mutations within the catalytic domain of gene-related kinases that spatially hinder drug binding while maintaining catalytic activity [80,81,86]. 4. Mutations in the active site of gene-related kinases that increase affinity for ATP, thereby rendering inhibitors that compete with ATP ineffective [87,88]. Based on monitoring and analyzing tumor resistance mutations, studies provide crucial insights and recommendations for formulating subsequent treatment strategies and making therapeutic decisions. Among these strategies, combining targeted therapies against subclonal mutations may represent the simplest and most effective approach to suppress the development of drug resistance.

Table 1. Tumor-associated genetic mutations in cfDNA.

Cancer Type	Stage	Sample	Technique	Genetic Mutations	Ref.
Colorectal cancer	Advanced	Plasma	BEAMing	APC, KRAS, PIK3CA, TP53	[89]
	Early to advanced	Plasma	ME-PCR	KRAS	[90]
Colorectal and breast cancer	Advanced	Plasma	WGS	Chromosomal alterations	[91]

Table 1. *Cont.*

Cancer Type	Stage	Sample	Technique	Genetic Mutations	Ref.
Ovarian cancer	Advanced	Plasma	TAm-Seq Digital PCR	TP53, PTEN, EGFR, BRAF, KRAS	[92]
	Early to advanced	Serum	Fluorescent-PCR	PIK3CA	[93]
Hepatocellular carcinoma	Early	Plasma	WGS	SNV	[94]
Non-small-cell lung cancer	Advanced	Plasma	ARMS-qPCR	KRAS	[95]
Breast and osteosarcoma	Advanced	Plasma and serum	Nested-real time PCR	Genomic alterations	[96]
Breast cancer	Advanced	Plasma	TAm-Seq and digital PCR	PIK3CA, TP53, structural variation	[97]
	Early to advanced	Plasma	BEAMing	PIK3CA	[98]

Abbreviations: WGS, whole-genome sequencing; SNV, single nucleotide variants.

Table 2. Mutations responsible for acquired drug resistance with subsequent treatment recommendations.

Cancer Type	Genetic Mutations	Subclonal Mutation	Acquired Drug Resistance	Corresponding Strategies	Ref.
Colorectal cancer	KRAS	Codon 12, 13, and 61	Cetuximab	Combination therapies targeting at least two different pathways for subclonal mutations.	[82]
		Q61H, G13D, G12D	Cetuximab	Blood-based non-invasive monitoring of KRAS mutant clones and early combined treatment with an MEK inhibitor.	[83]
	NRAS	Positions 12 and 61	Cetuximab Panitumumab	An EGFR-MEK concomitant blockade (cetuximab and pimasertib) induced prolonged ERK inhibition.	[74,83]
	BRAF	Position 600			
NSCLC	EGFR	T790M	Gefitinib Erlotinib	Use irreversible inhibitors that bind covalently or reversible inhibitors that bind with a sufficient affinity to outcompete ATP.	[87,99]
		T790M mutation and MET amplification	Gefinitib Erlotinib	Combined PI3K and MEK inhibitors, T790M-specific EGFR inhibitors, or combinations of anti-EGFR therapies.	[84]
	PIK3CA	E545K	Paclitaxel	Paclitaxel combined with mTOR inhibitors (rapamycin or its analogues)	[99,100]
	ALK	C1156Y, L1196M	Crizotinib	Determine the crystal structure of the ALK kinase domain with C1156Y or L1196M mutations and develop new-generation ALK inhibitors	[86]
	KRAS	G12C	Adagrasib Sotorasib	Combined inhibition of $KRAS^{G12C}$ and mTORC1 (RMC-4998 and RMC-6272, RM-018 and RMC-6272)	[101]

Table 2. *Cont.*

Cancer Type	Genetic Mutations	Subclonal Mutation	Acquired Drug Resistance	Corresponding Strategies	Ref.
Melanoma	MEK1	C121S	Vemurafenib	Gene amplification or altered pharmacokinetics: dose escalation; develop new drugs to circumvent on-target kinase resistance mechanisms.	[80]
	PDGFRβ upregulation and NRAS mutations	Q61K	Vemurafenib	Stratify patients with drug-resistant relapses and combine MEK activation inhibitors and kinase activity inhibitors.	[85]
	^{V600E} BRAF	Amplification	Vemurafenib	Combination with MEK1/2 inhibitor (Selumetinib)	[102]

Abbreviations: NSCLC, non-small-cell lung cancer; mTOR, mammalian target of rapamycin pathway; RMC-4998, orally bioavailable active-state KRAS^{G12C} inhibitor; RMC-6272, mTORC1-selective bi-steric inhibitor; and RM-018, active-state RAS^{G12C} inhibitors.

3.1.2. Combined with Subclonal Mutation Inhibitors

The exploration of mechanisms underlying subclonal mutation resistance holds profound clinical implications. Overcoming subclonal mutations that drive drug target amplification may be achieved by escalating the dosage of the targeted agent. Studies in chronic myeloid leukemia have demonstrated that increasing imatinib dosage can lead to secondary remission [103,104]. Moreover, when drug target amplification or other types of mutations lead to changes in drug metabolism, increasing the dose is also a candidate. Nevertheless, dose escalation is strictly limited by adverse drug reactions, and is basically ineffective when downstream pathways or bypass resistance pathways are activated. Therefore, the optimal approach involves combining subclonal mutation inhibitors to precisely target resistance mutations.

In numerous studies involving drugs listed in Table 2, subclonal mutations induced by targeted therapies have been identified as contributors to tumor resistance against targeted inhibitors, among which mutations in KRAS, NRAS, and BRAF are more typical. Regardless of the specific mutation type, resistant cells typically exhibit activation of the MAPK pathway or the PI3K/AKT/mTOR pathway [74,82,83,85,99–102]. This activation persists even after blocking the corresponding receptor initially targeted by the therapy. The sole inhibition of downstream signaling pathways or bypass pathways does not effectively hinder the growth of resistant cells in vivo or in vitro. RNA interference screening has demonstrated that the simultaneous inhibition of the original targeted receptor, along with suppression of downstream and bypass pathways, is crucial to curbing tumor resistance, proliferation, and metastasis [74]. Several studies have highlighted that the combined administration of inhibitors targeting these downstream and bypass pathways significantly impedes the growth of resistant tumor cells. This approach has successfully led to tumor regression, and in some cases, complete remission, without notable side effects [74,83,101].

In contrast to pathway activation, mutations at the active site of alternate kinases can enhance the target's affinity for ATP, thereby reducing the efficacy of kinase inhibitors that compete with ATP binding. To overcome such subclonal mutations, covalently bound irreversible inhibitors or inhibitors with substantially higher affinity than ATP are necessary [87,88,99]. However, once bound covalently, these inhibitors no longer maintain a reversible competitive equilibrium with ATP, potentially leading to off-target effects and toxicity, necessitating further in-depth studies [88].

In contrast to previous scenarios, mutations in the catalytic domain of gene-associated kinases can lead to drug resistance even when catalytic activity remains intact, which arises because the mutated structure creates steric hindrance that prevents drug binding to the protein pocket. This mechanism has been observed across various tyrosine kinases, includ-

ing imatinib, erlotinib, gefitinib, and crizotinib [86,105–107]. Notably, gatekeeper mutations affecting a conserved threonine residue near the active site of the kinase significantly impair binding with most tyrosine kinase inhibitors, such as the typical mutations of threonine at position 315 of ABL and threonine at position 790 of EGFR [108–110]. For this type of subclone mutation, it is necessary to analyze the crystal structure of the kinase domain after mutation and design a new generation of inhibitors by computer simulation in order to inhibit tumors carrying such subclone mutations effectively.

3.1.3. Model Prediction

In addition, to further circumvent the problem of subclonal resistance, various mathematical models have been developed, and new methods of ranking resistant subclones according to the time of emergence describe the full spectrum of resistance mutations present in metastatic lesions. This method can predict how many drug-resistant clones will arise in each lesion and provide precise quantification of the relative sizes of these resistant subclones. This model aims at multiple metastatic lesions in patients, amplifying the heterogeneity of drug-resistant mutations, and assisting second-line treatment with known resistant mutations for further drug planning (Figure 2H–J) [75,111]. However, in clinical practice, although non-sequential dual or triple therapy improves the survival and prognosis of most patients, the cytotoxicity of the combination therapy may complicate resistant mutations in individual cases, so the medication plan needs to be determined by the clinical situation [112,113].

3.1.4. Cancer Vaccines and Adoptive T-Cell Therapy

Vaccines and adoptive T-cell therapy approaches targeting clonal neoantigens create new possibilities for solving tumor resistance. Previous studies have demonstrated a relationship between clonal neoantigen burden and overall survival in primary lung adenocarcinoma by comprehensive analysis of intratumoral heterogeneity and neoantigen burden, which also provides evidence that the $CD8^+$ T cell population (expressed high levels of PD-1) can recognize clonal neoantigens present in all cells of a tumor [114]. A personalized vaccine regimen consisting of chimpanzee adenovirus (ChAd68) and mRNA (samRNA), combined with nivolumab and ipilimumab, have also induced neoantigen $CD8^+$ T cell responses in advanced metastatic tumors, suggesting that shared neoantigen vaccines isolated from common oncogenic driver mutations provide a viable template for "off-the-shelf" vaccines (Figure 2K) [76]. In the latest study, the safety and tolerability of a therapeutic vaccine encoding 20 shared neoantigens, consisting of ChAd68, samRNA, and immune checkpoint inhibitors (ipilimumab and nivolumab), was evaluated. Studies have shown that the vaccine drives tumor-specific T cell responses, increases $CD8^+$ T cells, expands neoantigen-specific effector memory T cells, and triggers T cell responses to HLA matching, thus achieving clinical benefits. The T cell response in the study was biased towards TP53, which matches the human leukocyte antigen encoded in the vaccine, indicating that a previously unknown hierarchy of neoantigen immunodominance may affect the therapeutic efficacy of multi-epitope shared neoantigen vaccines. This prompts us to generate targeted "off-the-shelf" vaccine libraries that can be used in combination or split to match tumor mutations or used for drug-resistant treatments in specific indications with high prevalence (Figure 2L) [77].

Generally, the significant overlap of genetic events associated with primary and acquired resistance supports clonal selection associated with tumor heterogeneity as a major determinant of therapeutic outcomes. Combining drugs targeting subclonal mutations to prevent convergent evolution, modeling quantitative cloning for adjuvant drug planning, utilizing clonal neoantigen vaccines, and adopting adoptive T-cell therapy are potential strategies for managing the evolution of cancer resistance and implementing early intervention. These approaches aim to enhance clinical benefits and extend survival rates.

3.2. Dismantle the Breeding Grounds of Drug Resistance

3.2.1. Normalization of Blood–Lymph Network

The concept of angiogenesis has been proposed for more than 50 years, but it was not until Professor Folkman proposed that anti-angiogenic substances can treat tumors in 1971 that anti-angiogenic treatment began [115]. In early studies, scientists believed that anti-angiogenic treatment would not produce severe drug resistance and cytotoxicity because it was based on "starving tumors" and targeted genetically stable vascular endothelial cells [116]. But even after harvesting some clinical benefit, patients still suffered from cytotoxicity which far exceeds expectations. For example, clinical trials of bevacizumab in HER2-negative metastatic BC demonstrated that it produced serious adverse reactions (hypertension and organ failure). As research matures, the strategy of "normalizing tumor blood vessels to improve drug and oxygen delivery" has been proposed [117]. Blood vessel normalization refers to restoring the disordered tumor blood vessels to a normal state (reduced blood vessel density, more regular blood vessel distribution, complete pericyte coverage, and increased tumor perfusion) through drug treatment, ultimately improving drug delivery efficiency and delaying drug resistance. In recent decades, scientists have appropriately restored the structural and functional defects of tumor blood vessels and enhanced the internal perfusion of tumors by continuously optimizing this method. Here, we outline three strategies for vascular normalization: employing vascular endothelial growth factor inhibitors, enhancing pericyte coverage, and reinforcing tight junctions.

In the 1980s, the vascular endothelial growth factor (VEGF) was discovered, and scientists believed it would be an important target for controlling tumor blood vessel growth [118]. In 1993, research on inhibitors of the VEGF showed that it effectively inhibited tumor growth (Figure 3A,B). Then, bevacizumab was developed as the first angiogenesis inhibitor and approved for marketing (Table 3) [119]. Subsequently, VEGF inhibitors such as olinvalumab, AK109, CTX-009 (ABL001), BAT-5906, sunitinib, and sorafenib were gradually launched. The effects of bevacizumab alone and in combination have been verified and evaluated in a variety of tumor models, and satisfactory clinical benefits have been achieved in recurrent or metastatic malignant tumors. For example, bevacizumab combined with paclitaxel, carboplatin, or sigitabine has been used in patients with bevacizumab-resistant recurrent epithelial ovarian cancer [120], metastatic breast cancer [121], and non-small-cell lung cancer [122], thus improving progression-free survival and overall response (Figure 3C). Clinical observations have also documented reductions in blood perfusion, vascular volume, microvessel density (MVD), interstitial fluid pressure (IFP), and permeability surface area product, alongside increases in drug delivery and the proportion of pericyte coverage on blood vessels [121–123]. Moreover, the use of Ziv-aflibercept and sunitinib in glioblastoma and glioma has demonstrated that inhibition of the VEGFR can decrease MVD and vascular diameter, enhance pericyte coverage, and reduce IFP, effectively promoting vascular normalization [124–127]. Small doses of VEGF inhibitors can balance the level of signals generated in blood vessels and reduce permeability by tightening cell–cell connections and recruiting pericytes, thereby restoring a normal vascular status and increasing tumor perfusion (Figure 3D) [123]. However, the application of VEGF inhibitors has been limited due to differences in xenogeneic therapy [128] (e.g., prostate cancer and pancreatic cancer are unresponsive to angiogenesis regulators, and tumors such as renal cell carcinoma are more sensitive to VEGF inhibitors), a narrow therapeutic "time window", and the occurrence of complications. Therefore, it is crucial to find effective and long-term stable vascular normalization strategies.

Pericytes are an essential component in maintaining vascular integrity, and tumor vessels often lack their coverage (Figure 4A,B) [129]. Thus, improving pericyte coverage can normalize blood vessels. Angiopoietins (Ang1, Ang2, Ang3, and Ang4) and their receptor Tie2 play a key role in the formation and remodeling of blood vessels. Studies have found that when Ang2 is knocked out in mice, the microvessel diameter of tumors (melanoma or Lewis lung cancer) in mice is reduced and the perivascular contour is more complete, which indicates that inhibiting Ang has potential therapeutic benefits (Figure 4C) [130,131].

At present, Ang inhibitors have been studied in preclinical studies, which reduce tumor angiogenesis and lymphangiogenesis and improve the efficacy of chemotherapy in colorectal, renal, ovarian, and lung cancer models. Moreover, without affecting Ang1-Tie2, the use of antibodies that promote the internalization of the Ang2-tie2 receptor complex can enhance the integrity of cell–cell junctions, thereby reducing vascular leakage (Figure 4E,F) [132]. Trebananib is a peptide-Fc fusion protein that inhibits angiogenesis by interfering with the binding of Ang1 and Ang2 to the Tie2 receptor. In a clinical phase III study, its combination with chemotherapy agents effectively improved the progression-free survival of patients with recurrent ovarian cancer (Figure 4G) [133]. Similarly, the VE-PTP inhibitor (AKB-9778) activates Tie2, which increases pericyte coverage, vessel diameter, and vessel density, and decreases vascular permeability in the tumor vasculature (Figure 4D) [134]. The up-regulation of Ang1 can also regulate tumor vascular morphology, reduce leakage and hypoxia, and restore blood flow [135].

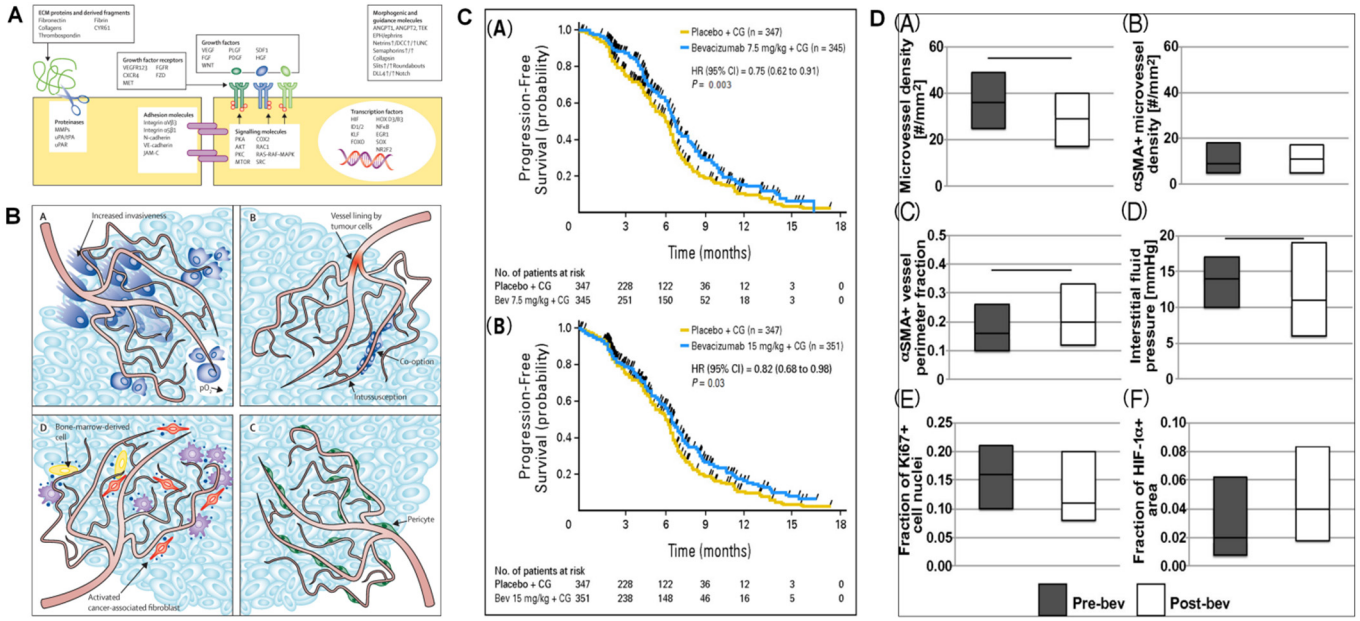

Figure 3. Employing vascular endothelial growth factor inhibitors. (**A**) A summary of some of the major molecules implicated in angiogenesis [128]. (**B**) Potential mechanisms of resistance to targeted VEGF therapy in cancer [128]. In established tumours, VEGF blockade aggravates hypoxia, which upregulates the production of other angiogenic factors or increases tumour cell invasiveness (a). Other modes of tumour vascularisation, including intussusception, vasculogenic mimicry, differentiation of putative cancer stem cells into endothelial cells, vasculogenic vessel growth, and vessel co-option, might be less sensitive to VEGF blockade (b). Tumour vessels covered by pericytes are less sensitive to VEGF blockade (c). Recruited proangiogenic bone-marrow-derived cells, macrophages or activated cancer-associated fibroblasts can rescue tumour vascularisation by production of proangiogenic factors (d). (**C**) A plot of the Kaplan–Meier estimates for progression-free survival (non-small-cell lung cancer) for the (a) 7.5 mg/kg bevacizumab (Bev) arm and the (b) 15 mg/kg bevacizumab arm compared with a placebo [122]. (**D**) The effect of a single injection of bevacizumab on the structural and functional markers of vascular normalization [123]. (a) Microvessel density decreased. (b) Bevacizumab did not affect the density of mature vessels. (c) Fraction of vessel perimeter associated with pericytes (αSMA+ cells), a marker that distinguishes between poorly and completely covered vessels, increased. (d) Interstitial fluid pressure, which is a functional measurement of vessel leakiness and lymphatic vessel dysfunction, decreased. (e,f) Histological markers of functional vascular normalization, Ki67 for proliferation and HIF-1α, did not change significantly. In order to distinguish the figure and subfigure, the subfigures' labels are replaced by lowercase letters in annotation.

Table 3. The role of VEGF inhibitors in the normalization of tumor blood vessels.

Cancer Type	Drug	Combination Therapy	Target	Corresponding Effects	Limitation	Ref.
Metastatic breast cancer	Bevacizumab	Paclitaxel	VEGF-A	Significantly prolonged progression-free survival as compared with paclitaxel alone and increased the objective response rate.	No change in overall survival.	[121]
NSCLC	Bevaci-zumab	Cisplatin Gemcitabine (CG)	VEGF-A	Combining bevacizumab (7.5 or 15 mg/kg) with CG significantly improved PFS and an objective response rate.	The overall incidence of serious adverse events was higher in the combination group than in the control group.	[122]
HER2-negative breast cancer	Bevaci-zumab	Adriamycin Cy-clophosphamide Paclitaxel (ACP)	VEGF-A	Bevacizumab combined with ACP showed superior anti-tumor activity in TNBC. Bevacizumab induced changes in the vascular structure and levels of circulating biomarkers indicative of vascular normalization in breast cancer.	Tumor regression from the VEGF blockade might be restricted to tumors with a sufficiently high MVD.	[123]
Glioblastoma	Ziv-aflibercept	γ radiation	VEGFR-2	The VEGFR-2 blockade can temporarily normalize the tumor vessel structure (pericyte and basement membrane coverage), leading to improved vascular function (tumor oxygenation) and an enhanced response to radiation therapy.	/	[124,125]
Glioma	Sunitinib	Temozolomide	VEGFR	Sunitinib decreased tumor IFP and increased temozolomide delivery. For mothiazole amine and PVC, it is closely relative to coverage, and its transmission efficiency is inversely proportional to the density of the collagen type IV basement membrane, showing that it can induce the normalization of tumor blood vessels.	/	[126,127]

Abbreviations: NSCLC, non-small-cell lung cancer; PFS, progression-free survival; TNBC, triple-negative breast cancer; MVD, microvascular density.

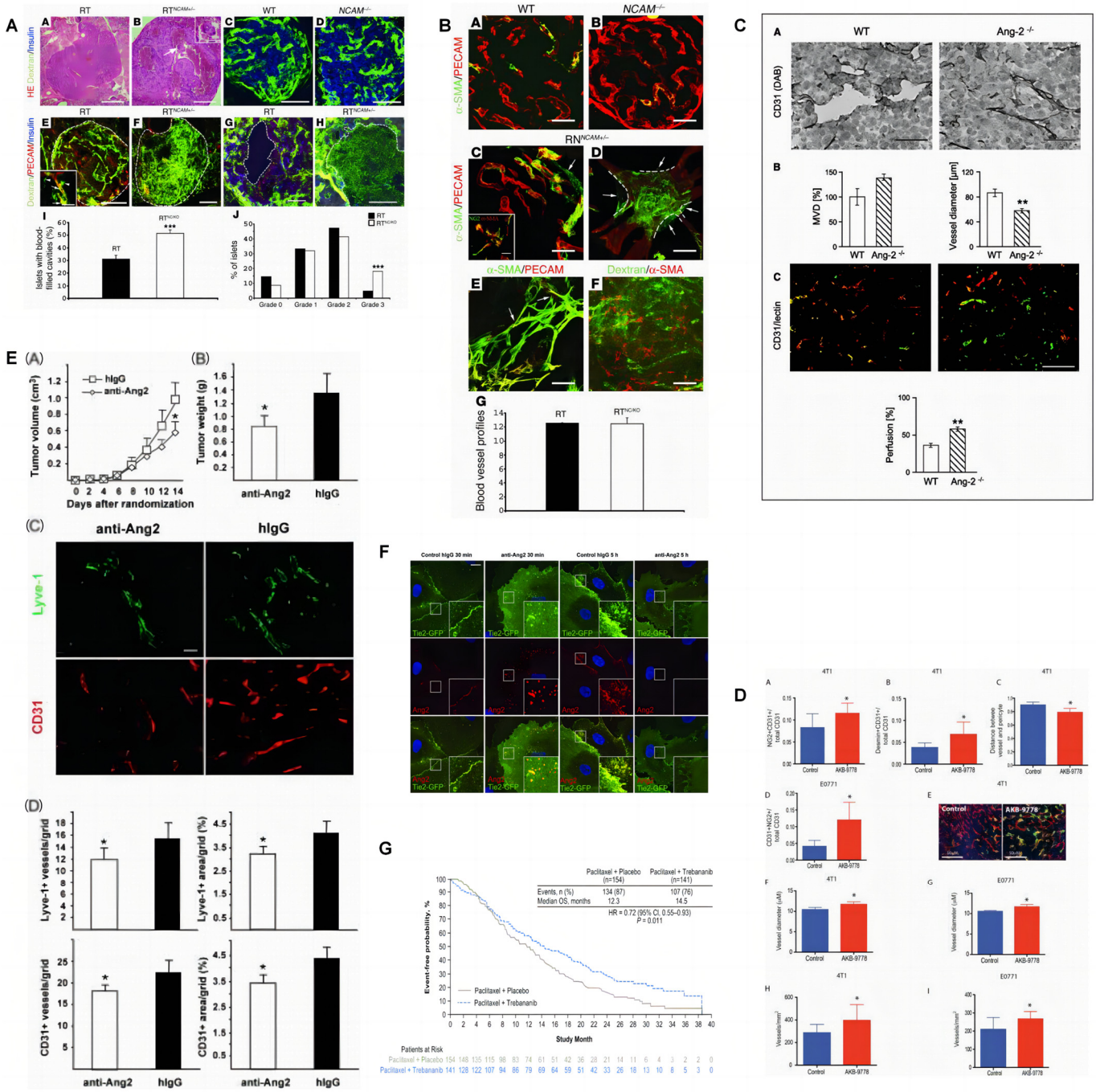

Figure 4. Enhancing pericyte coverage. (**A**) Neural cell adhesion molecule deficiency induces increased tumor blood vessel leakage during β tumor cell progression [129]. NCAM deficiency induces increased Pancreas sections from 8-week-old RT (a) and $RT^{NCAM+/-}$ mice (b) were stained with H&E. (b) Isolated cell clusters were specifically found inside blood-filled cavities within $RT^{NC/KO}$ islets (arrow). Inset in (b) shows a higher magnification of the isolated cell cluster. (c–h) Pancreas sections of mice perfused with FITC-dextran (green) were double-immunostained with antibodies against PECAM (red) and insulin (blue). (c,d) Islets from WT (c) and $NCAM^{-/-}$(d) mice. (e–h) Angiogenic islets from 8-week-old RT (e,g) and $RT^{NCAM+/-}$(f,h) mice. The islet area is indicated by dashed lines, and extravascular and intravascular FITC-dextran is indicated by arrowheads and arrows, respectively, in inset in (e). Dashed lines in g and h mark blood-filled cavities. FITC-dextran specifically leaked into $RT^{NC/KO}$ blood-filled

cavities (h). (i) The percentage of islets containing blood-filled cavities was higher in $RT^{NC/KO}$ compared with RT mice at 8 weeks of age (χ^2 test, *** $p < 0.001$). (j) Distribution of RT and $RT^{NC/KO}$ islets at 8 weeks of age according to their vessel leakage (grades 0–3, where grade 3 includes islets with most extensive leakage). (**B**) The pathological organization of periendothelial α-SMA^+ cells correlates with increased tumor vessel leakage in $RT^{NC/KO}$ angiogenic islets [129]. Pancreas sections from 8-week-old mice were double-immunostained with antibodies against PECAM (red) and α-SMA (a–e, green; f, red). In WT (a) and $NCAM^{-/-}$ (b) islets, α-SMA^+ cells were closely attached to the endothelium. Premature abnormal organization of periendothelial α-SMA^+ cells, including detachment of α-SMA^+ cells from endothelial cells (arrow in c) and multiple layers of α-SMA^+ cells with an apparent loose attachment to the endothelium (d), and presence of fibroblastlike α-SMA^+ cells in $RT^{NCAM+/-}$ angiogenic islets (e), were observed in $RT^{NCAM+/-}$ islets. The dashed lines and arrows in d indicate the borders of the endothelium and α-SMA^+ cells stretching away from the vessel, respectively. (f) Pancreas section of an 8-week-old $RT^{NCAM+/-}$ mouse perfused with FITC-dextran (green), immunostained with anti–α-SMA (red). Increased leakage correlated with severely disorganized α-SMA^+ periendothelial cells. The inset in (c) shows coexpression of NG2 (green) and α-SMA (red). (g) Analysis of blood vessel density revealed no difference between RT and $RT^{NC/KO}$ islets. (**C**) The effect of host-derived Ang-2 deficiency on MVD (a,b), the diameter of intratumoral microvessels (a,b), and perfusion (c) in Lewis lung carcinoma tumors [130]. (**D**) Structural changes within established primary tumor vessels invoked by vascular endothelial protein tyrosine phosphatase (VE-PTP) inhibition [134]. (a) Colocalization of CD31-positive area (endothelial cells) and NG2-positive area (perivascular cells) (* $p = 0.05$ by two-sided t test; n = 6 per group) in 4T1 tumors. (b) Colocalization of CD31-positive area (endothelial cells) and desmin-positive area (perivascular cells) (* $p = 0.01$ by two-sided t test; n = 6 per group) in 4T1 tumors. (c) Mean distance between desmin-positive pericytes and CD31 = positive endothelial cells in microns (* $p < 0.01$ by two-sided t test; n = 6 per group) in 4T1 tumors. (d) Colocalization of CD31+ area (endothelial cells) and NG2+ area (perivascular cells) (* $p = 0.05$ by two-sided t test; n = 6 per group) in E0771 tumors (* $p < 0.01$ by two-sided t test; n = 6 per group). (e) Enhanced vascular pericyte coverage in AKB-9778–treated tumors (right panel) compared with control-treated tumors (left panel) (red: CD31; green: NG2; blue: DAPI). (f,g) Vessel diameter in control vs. AKB-9778–treated 4T1 (f) and E0771 (g) tumors (f: * $p < 0.01$ by two-sided t test, n = 6 per group; g: * $p < 0.01$ by two-sided t test, n = 6 per group). (h,i) Vessel density in control vs AKB-9778–treated 4T1 (h) and E0771 (i) tumors (h: * $p = 0.05$ by two-sided t test, n = 6 per group; i: * $p = 0.05$ by two-sided t test, n = 6 per group). (**E**) Ang2-blocking antibodies inhibit primary tumor growth, angiogenesis, and lymphangiogenesis [132]. (a) Growth curves of LNM35 primary tumors in nu/nu mice treated with the Ang2-blocking antibodies or hIgG control, n = 8 in both groups. (b) Tumor weights at excision 16 days after implantation, $p = 0.002$. Student's *t* test. (c) Representative immunohistochemical images of LYVE-1- and CD31-stained tumor sections. (d) Quantification of densities and area fractions of Lyve-1-positive lymphatic vessels and of CD31-positive blood vessels from at least five histological sections, $p = 0.013$ and 0.019, respectively. Student's *t* test. (**F**) The Ang2-blocking antibody induces internalization of the Ang2-Tie2 complexes, leaving Ang1-Tie2 complexes intact at endothelial cell–cell junctions [132]. (**G**) The overall survival in patients with ascites at baseline (trebananib plus weekly paclitaxel in recurrent ovarian cancer) [133]. In order to distinguish the figure and subfigure, the subfigures' labels are replaced by lowercase letters in annotation.

In addition, VE-cadherin is the main component of endothelial cell-strengthened tight junctions, and its inhibition can increase vascular permeability [136]. The drug CU06-1004 enhances the endothelial barrier through the Camp/Rac/Cortactin pathway, forming cortical actin rings and thereby upregulating adherens junctions such as VE-cadherin. In both lung cancer and melanoma models, CU06-1004 improved the link integrity and perfusion efficiency of the tumor vasculature and reduced vascular penetration (Figure 5A,B). When it is combined with cisplatin or carboplatin, its chemotherapy efficacy is also improved due to vascular normalization [137].

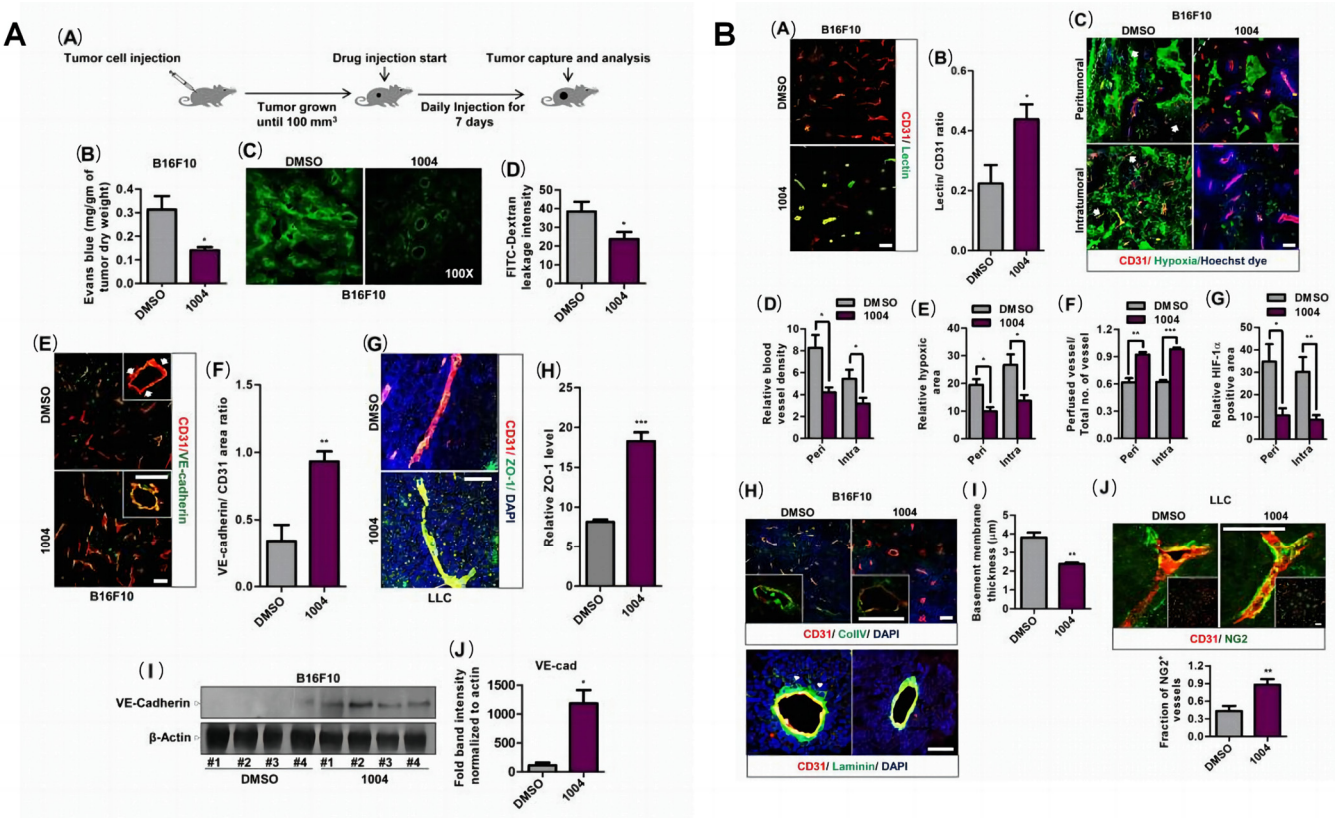

Figure 5. Reinforcing tight junctions. (**A**) CU06-1004 reduces vascular leakage with a concomitant increase in junction integrity in tumor blood vessels [137]. (a) Schematic plan for the administration of Sac-1004 or control (DMSO) to tumor-bearing mice. (b) B16F10 tumor-bearing mice (n = 5) were injected with Sac-1004 or control as in (a) and tumor vascular leakage was quantified by the Evans blue method. (c) Vascular leakage was assessed by FITC-dextran. (d) Images shown in (c) were quantified using ImageJ software. (e) Immunofluorescence staining of B16F10 tumor sections, treated with Sac-1004 or control, for CD31 and VE-cadherin. Arrows indicate discontinuity in VE-cadherin staining. (f) Quantification of immunofluorescence images shown in (e) using Multi Gauge software (n = 5). (g) LLC tumor sections, treated with Sac-1004 or control were costained for CD31, ZO-1 and DAPI. (h) Images shown in (g) were quantified using ImageJ software (n = 5). (i) Western blot analysis of B16F10 tumors treated with Sac-1004 or control for VE-cadherin. (j) VE-cadherin and actin blots from (i) were quantified using ImageJ software. * $p < 0.05$; ** $p < 0.01$; *** $p < 0.001$ (Student's *t*-test). (**B**) CU06-1004 improves vascular perfusion, alleviates hypoxia, and normalizes tumor blood vessels in tumors [137]. (a) Immunofluorescence staining of B16F10 tumor sections (n = 5), treated with Sac-1004 or control, for CD31 and tomato lectin. (b) Images shown in (a) were quantified using Image J software. (c) Immunohistochemical analysis of B16F10 tumor sections (n = 5) for CD31, hypoxia, and vascular perfusion (Hoechst dye) in the peritumoral and intratumoral zone. Arrows indicate non-perfused vessels. (d–f) Quantification of immunofluorescence images shown in (c) with Multi Gauge software. (g) Quantification of HIF-1α positive area using Multi Gauge software. (h) B16F10 tumor sections (n = 5), treated with Sac-1004 or control, were stained for CD31 and ColIV (up)/laminin (bottom). Arrowheads indicate the point of detachment between basement membrane and endothelial cells. (i) Quantification of basement membrane thickness in B16F10 tumor vessels shown in (h) using Multi Gauge software. (j) Immunofluorescence staining of LLC tumor sections (n = 5) for CD31 and NG2. Quantification was done using Multi Gauge software. * $p < 0.05$; ** $p < 0.01$; *** $p < 0.001$ (Student's *t*-test). In order to distinguish the figure and subfigure, the subfigures' labels are replaced by lowercase letters in annotation.

In the previous section, we mentioned that the stress generated in the early stage of tumor proliferation will mechanically compress the blood vessels and lymphatic vessels

inside of the tumor. When the tumor nutrients are depleted, blood perfusion increases in the previously compressed vessels, but lymph flow in the lymphatic vessels does not resume [34,138]. At this time, to promote the metastasis of shed cancer cells, the tumor enhanced the contractility and pumping frequency of peripheral lymphatic vessels. There are two main strategies for lymphatic therapy: inhibiting lymphangiogenesis or manipulating the lymphatic system to promote the initiation of the tumor immune response. Simply inhibiting lymphangiogenesis is effective in preventing tumor metastasis, but it does not contribute much to intratumoral drug delivery. Therefore, when the normalization of intratumoral lymphatic vessels and the inhibition of peripheral tumor lymphangiogenesis are carried out at the same time, more therapeutic benefits will be harvested.

Studies have shown that by using the tumor-secreted vascular endothelial growth factor receptor 3 immunoglobulin fusion protein (VEGFR-3-Ig) as a decoy receptor for VEGF-C and VEGF-D, intratumoral lymphatic proliferation and lymph node metastasis will be reduced in mice (Figure 6A,B) [139,140]. Similarly, the results of studies with neutralizing antibodies against VEGFR-3 have shown reduced tumor-associated lymphangiogenesis, tumor growth, and lymph node metastasis in mice (Figure 6C,D) [141–143]. Therefore, although there is no relevant inhibitor designed for the lymphatic pathway at present, the method of neutralizing the downstream effectors of VEGFR-3 in the form of inhibitors may achieve the simultaneous advancement of the above two points.

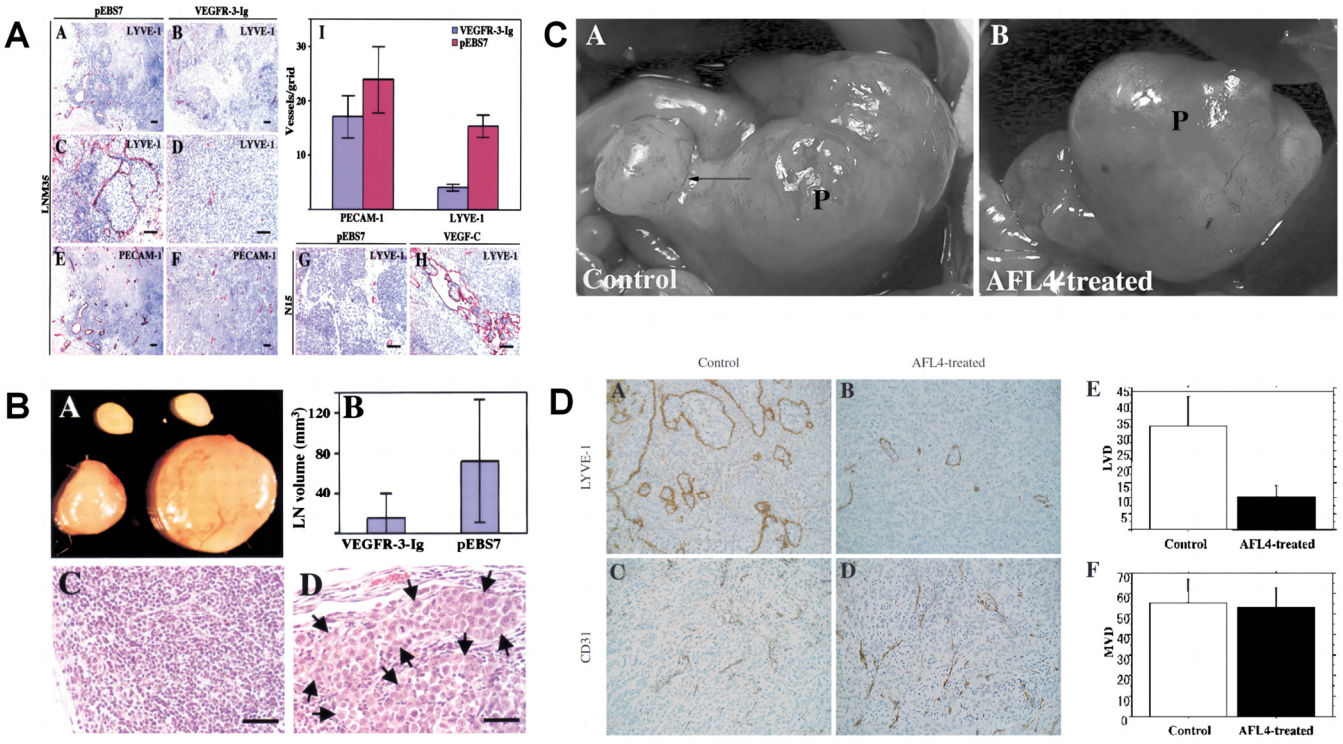

Figure 6. Normalizing intratumoral lymphatics while inhibiting peripheral tumor lymphangiogenesis. (**A**) The inhibition of tumor lymphangiogenesis by VEGFR−3−Ig (blood and lymphatic vessels in the LNM35 and N15 tumors) [139]. Immunohistochemical staining is shown for LYVE-1 (a–d,g,h) to identify lymphatic vessels and for PECAM-1 (e,f) to identify both blood and lymphatic vessels. (a,c,e) Sections of the control LNM35/pEBS7 tumors. (b,d,f) Sections from the LNM35/vascular endothelial growth factor receptor−3−Ig (VEGFR−3−Ig) tumors. (g,h) Sections of the N15/pEBS7 and N15/VEGF−C tumors, respectively. (i) LYVE-1-stained or PECAM−1−-stained vessels in three microscopic fields of the highest vessel density were counted, and the results were compared by use of the unpaired t test. (**B**) The suppression of axillary lymph node metastasis by VEGFR−3−Ig [139]. (a) Typical lymph nodes in mice

bearing the vascular endothelial growth factor receptor 3 Ig (VEGFR-3-Ig) tumors (upper pair) and control LNM35 tumors (lower pair). (b) Lymph node (LN) volume and 95% confidence intervals ($p = 0.070$). (c,d) Histologic staining of lymph node sections from mice with the VEGFR−3−Ig−overexpressing and control tumors, respectively. Arrows = tumor cells in the lymph node. (**C**) The inhibition of the metastatic spread of orthotopic gastric AZL5G tumors by the systemic administration of anti−VEGFR−3 antibodies (AFL4) [143]. (a) Control mouse (P; primary tumor, arrow; metastatic lymph node). (b): AFL4−treated mouse (P; primary tumor). (**D**) An assessment of lymphatic and blood vessel density in control and AFL4−treated mice [143]. Immunohistochemistry of primary tumors for LYVE−1 (a,b) and CD31 (c,d) and schema of the vessel counts (e,f). Compared with the control group, the number of LYVE−1−positive lymphatic vessels (LVD) in the primary tumors in the AFL4−treated group is dramatically decreased (e, $p < 0.05$). In contrast, CD31−positive LYVE−1−negative microvessel density (MVD) was not significantly different between the control group and the AFL4−treated group (f, $p = 0.84$). In order to distinguish the figure and subfigure, the subfigures' labels are replaced by lowercase letters in annotation.

In addition, recent studies have highlighted the therapeutic potential of the immunomodulatory capacity of the lymphatic system for lymphatic vessel normalization. VEGF-C-induced lymphangiogenesis enhanced adoptive T cell therapy and anti-PD-1 therapy in melanoma model studies, and the enhanced lymphangiogenesis depended on CCR7 signaling and the local activation of naive T cells, as the CCR7 blockade reversed VEGF-C enhancement (Figure 7A,B) [144]. Similarly, VEGF-C-mediated lymphangiogenesis also improved therapeutic efficacy by anti-PD-1/CTLA-4 combination therapy in ectopic brain tumor mice model studies, and this response was abolished by the CCL21/CCR7 blockade, indicating that VEGF-C enhanced therapy through the CCL21/CCR7 pathway (Figure 7C,D) [145]. Based on these studies, VEGF-C-mediated lymphangiogenesis may enhance immunotherapy in the tumor setting, such as the enhancement of adoptive T cell [144] and $CD8^+$ T cell [146] therapy.

3.2.2. Normalization of Extracellular Matrix

Even if the function of the blood–lymphatic network has been corrected, extracellular matrix obstacles still can hinder drug delivery and efficacy, so the normalization of the matrix still matters. As mentioned before, the penetration of the drug into the tumor depends on tumor stiffness and the volume fraction of extracellular matrix components, especially the content of collagen, glycoproteins, and proteoglycans. To reduce resistance, scientists have tried to degrade these components. It has been found that the injection of bacterial collagenase into stiff collagen tumors, such as MU89 melanoma, increases the diffusion volume of drug macromolecules by a factor of two (Figure 8A,B) [147]. However, the systemic administration of bacterial collagenase is not clinically practical due to the systemic distribution of collagen, so the study of relaxin and matrix metalloproteinases (MMP1 and MMP8) for the degradation of the collagen matrix has been attempted. After 2 weeks of treatment with relaxin, the collagen matrix in the desmoplastic tumor was reorganized, and the permeability of the drug macromolecules was significantly increased [148]. The ectopic expression of MMP1 and MMP8 also significantly increased the distribution of macromolecules, reduced the level of glycosaminoglycans, and improved drug permeability (Figure 8C,D) [149]. In addition, several retrospective studies have shown improved survival in patients with lung, renal, and pancreatic ductal cancers treated with angiotensin II receptor blockers (ARBs) or angiotensin-converting enzyme inhibitors, associated with reduced collagen production by blocking transforming growth factor β activation [150–152]. In subsequent studies, the blockade of transforming growth factor β signaling was shown to normalize blood vessels and the collagen matrix in a mouse mammary gland model and to effectively improve the therapeutic effect of doxorubicin (Figure 8E–G) [153,154].

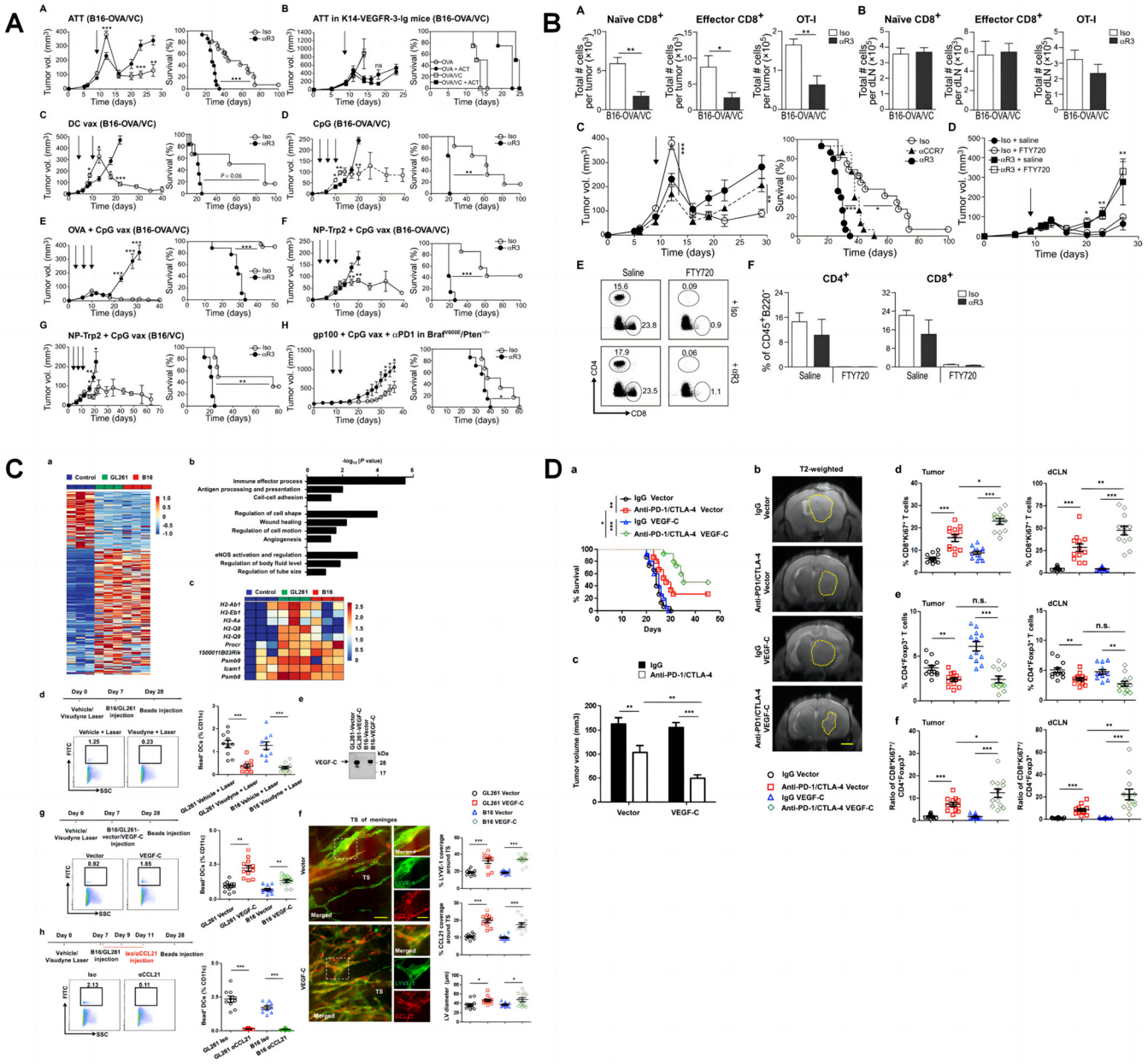

Figure 7. The therapeutic potential of lymphatic system immunomodulatory capacity for lymphatic normalization. (**A**) VEGF−C/VEGFR-3 signaling increases the responsiveness of melanoma to immunotherapy [144]. Tumor growth and survival of three different melanoma models treated with control (Iso) or aR3-blocking antibodies receiving different immunotherapies (arrows indicate times of administration). (a,b) B16-OVA/VC tumors treated with ATT in (a) WT ($n \geq 15$) and (b) K14−VEGFR−3−Ig mice that lack dermal lymphatics (n = 4). (c–f) B16−OVA/VC tumors in WT mice treated with (c) ex vivo activated DCs (DC vax; n = 6), (d) 50 mg of CpG (n = 6), (e) 10 mg of OVA + 50 mg of CpG ($n \geq 8$), and (f) 2 mg of Trp2 peptide−conjugated nanoparticles (NP-Trp2) + 50 mg of CpG (n = 7). (g) B16/VC tumors treated with NP-Trp2 + 50 mg of CpG (n = 6). (h) Tamoxifen-induced tumors in $Braf^{V600E}/Pten^{-/-}$ mice treated with CpG + gp100 peptide (days 8 and 12) and anti−PD−1 antibody (day 12 and every 4 days thereafter). Each panel shows data from one (b–d,f,g), two (e), or three (a) independent experiments. * $p < 0.05$, ** $p < 0.01$, *** $p < 0.001$ by two-tailed Student's *t* test for growth curves and log-rank (Mantel-Cox) test for comparing survival curves. (**B**) The increased efficacy of immunotherapy in lymphangiogenic B16 melanomas depends on CCR7 signaling before therapy and

the local activation and expansion of TILs after therapy [144]. (a,b) B16-OVA/VC tumor–bearing mice treated with control IgG (Iso) or anti−VEGFR−3 (aR3)–blocking antibodies were euthanized 3 days after ATT, and tumor single-cell suspensions were analyzed by flow cytometry (n = 5). Quantification of overall naïve $CD8^+$ ($CD45^+$ $CD8^+$ $CD44^-$ $CD62L^+$), effector $CD8^+$ ($CD45^+$ $CD8^+$ $CD44^+$ $CD62L^-$), and OT-I ($CD45^+$ $CD8^+$ $CD45.1^+$) T cells (a) in the tumor and (b) in the dLNs. (c) Tumor growth and survival curves of B16-OVA/VC tumor−bearing mice treated with anti-CCR7 (aCCR7), control IgG (Iso), or aR3 antibodies combined with ATT on day 9. CCR7 blockade was performed only before ATT (days 0, 3, and 6) (data pooled from two or more independent experiments, n ≥ 15 total). (d) Tumor growth curves of B16−OVA/VC tumor–bearing mice treated with control IgG (Iso) or aR3 antibodies received daily injections of the small molecular S1P inhibitor FTY720 starting on the same day as ATT was performed (day 9) (n ≥ 5). Statistics show differences between Iso + FTY720 and aR3 + FTY720 by one-way ANOVA. (e) Representative flow cytometry plots and (f) quantification of circulating $CD4^+$ and $CD8^+$ T cells (after B220 exclusion) in blood 26 days after tumor inoculation. * $p < 0.05$, ** $p < 0.01$, *** $p < 0.001$ by two−tailed Student's t test or one−way ANOVA and log-rank (Mantel−Cox) test for survival curves. (**C**) Dorsal MLVs are the main route for immune cell entry to draining CLNs [145]. (a) Heat map of DEGs (Up, 219; Down, 100; power > 0.4). (b, c) Gene sets involved in lymphatic remodeling, fluid drainage, as well as inflammatory and immunological responses as shown by the representative upregulated pathways in GL261 tumor-associated and B16 tumor-associated MLECs compared to control MLECs (b), and heat map of DEGs enriched in the antigen processing and presentation pathway (c). (d) Left panels, treatment scheme and representative flow cytometry dot plots of DC trafficking from GL261 tumors to dCLNs in mice treated with Vehicle + Laser or Visudyne + Laser, determined by the quantity of $CD11c^+MHCII^+FITC^+$ cells in the dCLNs 24 h after intratumoral injection of FITC-labeled latex beads. Right panel, quantification of $Bead^+$ DCs in the dCLNs of mice treated with Vehicle + Laser or Visudyne + Laser. (e) Immunoprecipitation of secreted VEGF−C protein (arrow) in conditioned medium from GL261-Vector, GL261-VEGF-C, B16-Vector, and B16−VEGF−C cells. (f) Left panels, LYVE-1 and CCL21 staining of MLVs in mice bearing Empty and VEGF-C-overexpressing GL261 tumors in the striatum (scale bars, 100 μm in wide-fields; 50 μm in insets). Right panels, quantification of the percentage area of LYVE-1 and CCL21 (n = 10). (g) Left panels, treatment scheme and representative flow cytometry dot plots of DC trafficking in the dCLNs of mice bearing GL261 tumors overexpressing Vector or VEGF−C. Right panel, quantification of $bead^+$ DCs in dCLNs (n = 10). (h) Left panels, treatment scheme and representative flow cytometry dot plots of DC trafficking in the dCLNs of GL261 tumor-bearing mice treated with CCL21 (αCCL21)- or IgG (Iso)-blocking antibodies. Right panel, quantification of $bead^+$ DCs in dCLNs (n = 10). * $p < 0.05$, ** $p < 0.01$, *** $p < 0.001$. (**D**) A high level of tumor-derived VEGF-C improves anti-PD-1/CTLA-4 efficacy [145]. (a) Survival of mice with striatal Vector- or VEGF-Coverexpressing GL2161 tumors following the administration of anti-PD-1/CTLA-4 or IgG controls (n = 15). (b) Representative T2-weighted single brain slices from mice with intracranial injection of GL261 cells overexpressing Vector or VEGF-C (n = 6). (c) Tumor volumes in mice with striatal injection of GL261 cells overexpressing Vector or VEGF-C (n = 6). (d,e) Quantification of $CD8^+Ki67^+$ T cells (d) and $CD4^+Foxp3^+$ T cells (e) as percentages of overall $CD45^+$ cells in tumors and in dCLNs on day 14 after inoculation (n = 12 in each). (f) Ratios of $CD8^+Ki67^+$ T cells to Tregs in tumors and in dCLNs. * $p < 0.05$, ** $p < 0.01$, *** $p < 0.001$. In order to distinguish the figure and subfigure, the subfigures' labels are replaced by lowercase letters in annotation.

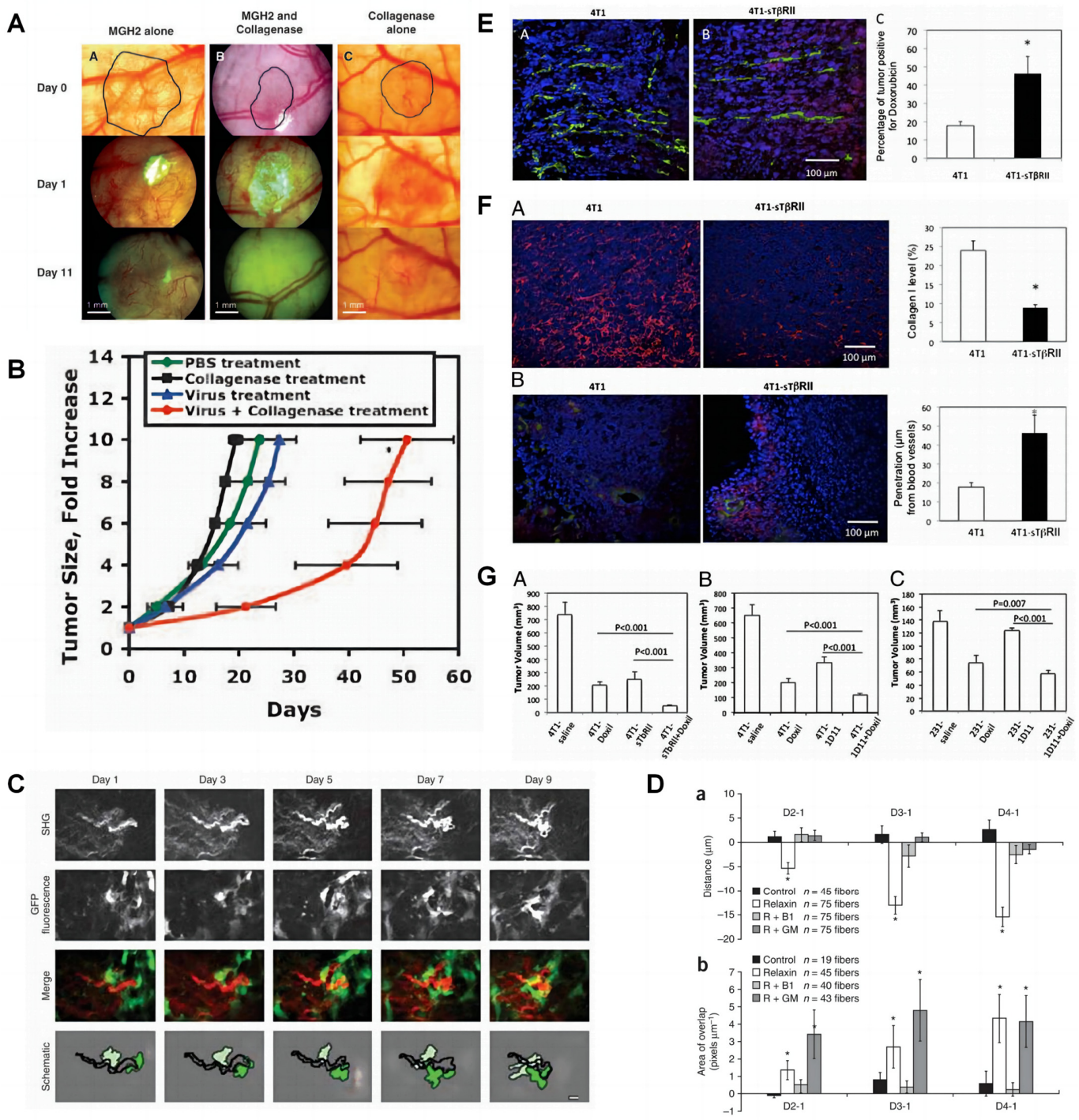

Figure 8. Normalization of the matrix. (**A**) The effect of collagenase on oncolytic viral therapy [147]. (**B**) The effect of collagenase on MGH2-induced tumor growth delay [147]. (**C**) The buckling of a collagen fiber in a relaxin-treated tumor [149]. (**D**) A quantitative analysis of collagen fiber length and the area of colocalization between stromal cells and fibers [149]. (a,b) The end-to-end fiber length (a) and the area of overlap between stromal cells and collagen fibers (b) was determined over 4 d in control groups as well as those treated with relaxin, relaxin and b1 integrin antibody (R + b1) and relaxin and GM6001 (R + GM). Shown are the averaged differences between day 1 and days 2 (D2-1), 3 (D3-1) and 4 (D4-1). * $p < 0.05$. (**E**) Blocking TGF-β signaling improves the intratumoral distribution

of doxorubicin in orthotopic mammary carcinoma models [153]. (a,b) Representative images of doxorubicin intratumoral distribution in 4T1 (a) and 4T1–sTβRII (b) tumors. Green, FITC–lectin-labeled perfused vessels; red, fluorescent doxorubicin; blue, DAPI. (c) Quantification of the fraction of tumor area positive for doxorubicin (n = 12 sections, with 3 sections per tumor). * $p < 0.001$. (**F**) Blocking TGF-β signaling decreases collagen I content and improves Doxil tissue penetration [153]. (a) Representative images and quantification of collagen I immunofluorescent staining in 4T1 and 4T1–sTβRII tumors. Red, collagen I staining; blue, DAPI (×20). (b) Representative images and quantification of Doxil intratumoral distribution in 4T1 and 4T1–sTβRII tumors. Green, FITC-lectin labeled perfused vessels; red, fluorescent doxorubicin; blue, DAPI (n = 12 sections, with 3 sections per tumor). * $p < 0.001$. (**G**) Blocking TGF-β signaling enhances Doxil efficacy in orthotopic mammary carcinoma models [153]. (a and b) Primary tumor growth of 4T1 and 4T1–sTβRII tumors, with or without Doxil treatment (a) and 4T1 (b) and MDA-MB-231 (c) tumors treated with saline (control), Doxil alone (9 mg/kg, weekly), 1D11 alone (5 mg/kg, three times a week), or combined Doxil and 1D11 (n = 8 in all groups). In order to distinguish the figure and subfigure, the subfigures' labels are replaced by lowercase letters in annotation.

3.3. Breaking the Safe Havens of Drug Resistance

Cancer metastasis typically signifies rapid disease progression, such as bone and brain metastases [155,156]. Brain metastases are characterized by the rapid expansion of intracranial tumors and the worsening of the primary tumor. However, due to the protective effects of the blood–brain barrier and the blood–tumor barrier, anticancer drugs often prove ineffective, presenting unique challenges in the treatment of intracranial tumors [63,155]. To overcome this barrier, various strategies are being explored or refined to enhance drug distribution and accumulation within the central nervous system's safe harbor. While both invasive and non-invasive methods are under investigation, this article focuses solely on non-invasive approaches, especially biochemical and physical therapies.

3.3.1. Biochemical Therapies

In previous studies, manipulating transport channels to improve the efficiency of transport across the BBB has been a common means to enhance drugs' effectiveness [62,157], for example, using transferrin and insulin receptors. Drug molecules link their ligands, which trigger endocytosis upon binding to their receptors and transport to the abluminal surface by vesicles, thereby achieving movement across the BBB [66,157,158]. However, because some receptors are widely distributed in the human body, off-target cytotoxicity has greatly limited the clinical application of this method. In addition, overcoming the efflux pump to pump out drugs can also increase the brain accumulation of tumor drugs. In clinical studies, the combination of anticancer drugs and transporter inhibitors has received great attention. In glioblastoma, the ATP-binding cassette (ABC) expressed by the BBB mediates the efflux of most drugs, with P-glycoprotein (ABCB1) and the breast cancer resistance protein (ABCG2 or BCRP) being dominant [159]. Studies have shown that ABCB1 and ABCG2 limit the BBB permeability of PARP inhibitors [160,161]. Hence, inhibiting ABCB1 and ABCG2 through elacridar effectively improved the efficacy of temozolomide (TMZ)/PARP inhibitor (veliparib) treatment for all glioblastoma patients (1.5-fold for TMZ, 5-fold for veliparib), and even PTEN-deficient glioblastoma becomes sensitive to TMZ (Figure 9A–C) [162]. Similarly, AET inhibitors (such as cyclosporine A, tariquidar, and valspodar) significantly modulated the activities of P-gp and BCRP in clinical models (Figure 9D), which increased the uptake of drugs in the rat brain and the distribution of drugs in the brain [60,163].

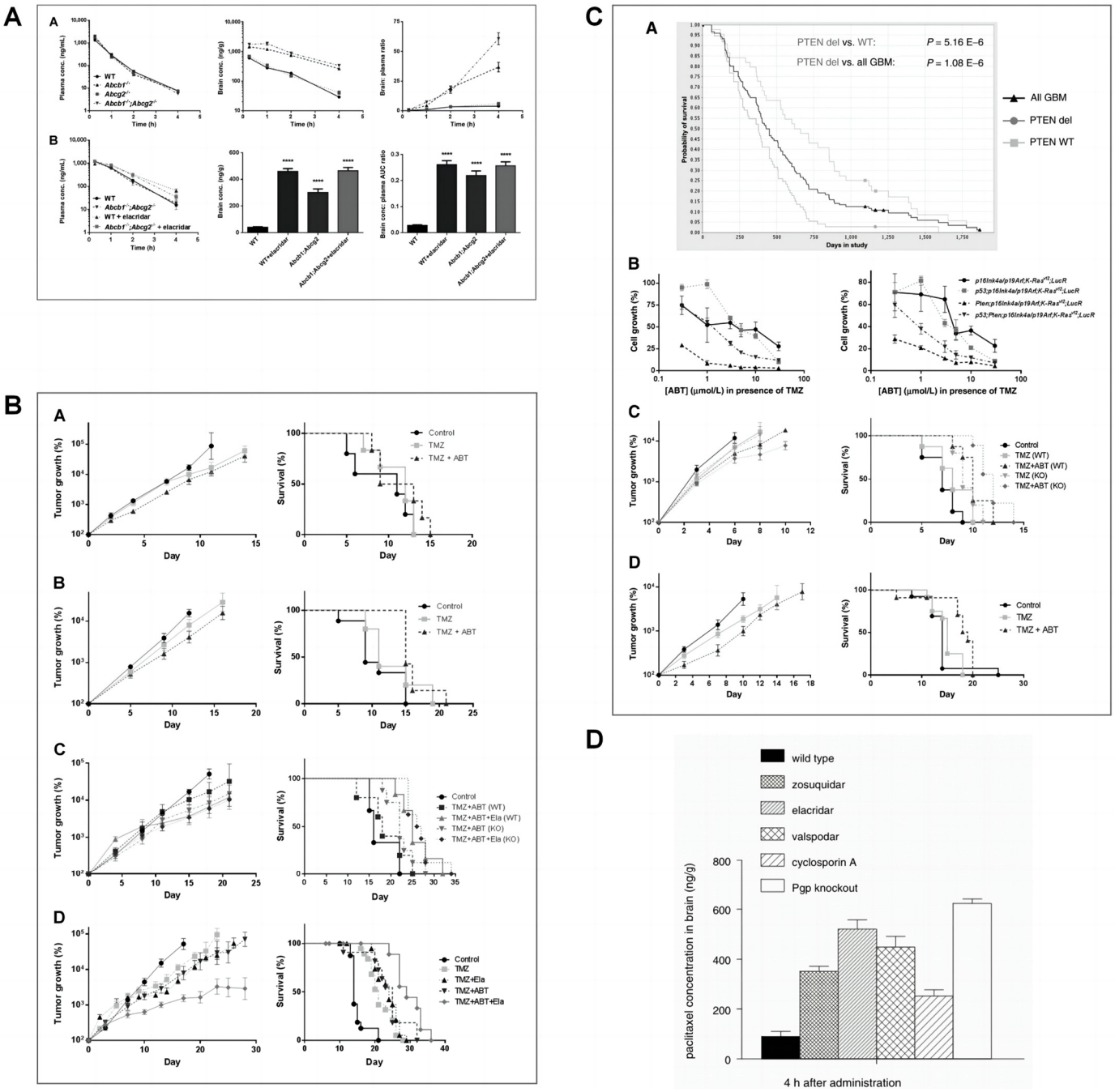

Figure 9. Biochemical therapies for breaking the safe haven. (**A**) The brain penetration of ABT-888 is limited by Abcb1 and Abcg2 [162]. (a) ABT-888 plasma concentrations, brain concentrations, and brain-to-plasma ratios following intravenous administration of 10 mg/kg of ABT-888 (n = 5/time point/strain). (b) ABT-888 levels following 10 mg/kg p.o. administered to wild-type and Abcb1a/1b$^{-/-}$; Abcg2$^{-/-}$ mice with/without co-administration of 100 mg/kg elacridar p.o. Blood samples were collected from the tail at 15 min, 1, 2, and 4 h (n = 8/strain). Brain samples were harvested at 4 h after drug administration. **** $p < 0.0001$ compared with wild-type. (**B**) The inhibition of Abcb1 and Abcg2 improve efficacy of ABT-888 + TMZ treatment [162]. (a) Efficacy of TMZ versus TMZþABT-888 treatment against intracranial p53; p16^{Ink4a}/p19^{Arf}; K-Ras^{v12}; LucR GBM652457 cells injected into wild-type mice. (b) Same setup but now injected into Abcb1a/1b$^{-/-}$; Abcg2$^{-/-}$(KO) mice. (c) Efficacy of TMZ + ABT-888 with and without

elacridar in both WT and KO mice. (d) Efficacy of TMZ or TMZ + ABT-888 with or without elacridar against (lentivirally induced) spontaneous p53; $p16^{Ink4a}/p19^{Arf}$; $K\text{-}Ras^{v12}$; LucR tumors. TMZ p.o. at 100 mg/kg every day alone or concurrently with ABT-888 p.o. at 10 mg/kg twice a day and/or elacridar p.o. at 100 mg/kg every day 15 min before TMZ for 5 days. Left, relative tumor growth curves. Right, Kaplan–Meier analysis of survival. (**C**) PTEN-deficient tumors are more sensitive to ABT-888 + TMZ treatment [162]. (a) Kaplan–Meier analysis of PTEN deletion ($\leq$1.8 copies) on overall survival of patients with glioblastoma. (b) Sensitivity (in vitro) of two panels of glioblastoma cell lines of different genetic backgrounds exposed to 100 µmol/L TMZ and increasing concentrations of ABT-888 for 5 days. (c) Efficacy of ABT-888 in combination with TMZ against Pten;$p16^{Ink4a}/p19^{Arf}$;$K\text{-}Ras^{v12}$;LucR GBM696677 cells injected intracranially into WT or Abcb1a/1b$^{-/-}$;Abcg2$^{-/-}$ (KO) mice and (d) spontaneous Pten;$p16^{Ink4a}/p19^{Arf}$; $K\text{-}Ras^{v12}$;LucR tumors. TMZ (100 mg/kg p.o. every day) alone or concurrently with ABT-888 (10 mg/kg p.o. twice a day) for 5 days. C and d (right), Kaplan-Meier analysis of survival. (**D**) The brain concentration of paclitaxel (10 mg/kg) in mice at 4 h after administration of paclitaxel alone and in combination with different (putative) inhibitors of Pgp (Pgp knockout mice were used as a reference for "complete" inhibition of Pgp) [163]. In order to distinguish the figure and subfigure, the subfigures' labels are replaced by lowercase letters in annotation.

3.3.2. Physical Therapies

Different from biochemical means, physical means induce the instability of tight junctions in the cerebral vasculature system through physical techniques, thereby generating intracranial high temperature and instantaneously (6–24 h) destroying the integrity of the BBB. Focused ultrasound (FUS) and circulating microbubbles (such as lipids and albumin) are classic physical therapies for destroying BBB. FUS disrupts the BBB or blood–brain tumor barrier in a thermo-mechanical manner by transmitting low-frequency ultrasound waves [57], while microbubbles change vascular permeability in response to the force exerted by ultrasonic pressure wave vibration (Figure 10A–C) [164]. Studies have shown that the simultaneous application of the above two technologies can generate shear stress in endothelial cells or activate signaling pathways that regulate barrier permeability, thereby inducing the transient opening of tight junctions in the blood–brain tumor barrier (Figure 10D–F) [165,166]. Multiple clinical studies have proven the feasibility of using FUS and microbubbles to improve chemotherapy agents' effectiveness. The effect of FUS combined with microbubbles on intracerebral TMZ treatment was tested in the BBB of nude mice implanted with U87 human glioma cells. The results showed that the local TMZ accumulation in the brain increased significantly (from 6.98 ng/mg to 19 ng/mg) after the transient opening of the BBB. TMZ degradation time in the tumor core also increased from 1.02 h to 1.56 h (Figure 10G,H) [167]. Similarly, in a healthy rabbit brain model, FUS-induced BBB opening increased the mean brain tissue and plasma drug concentrations of TMZ by 21% and irinotecan by 178% [168]. In addition to the above advantages of significantly improving drug brain distribution and accumulation, FUS can also control the size of the BBB opening through acoustic pressure and predict this using cavitation detection (Figure 10I,J) [169].

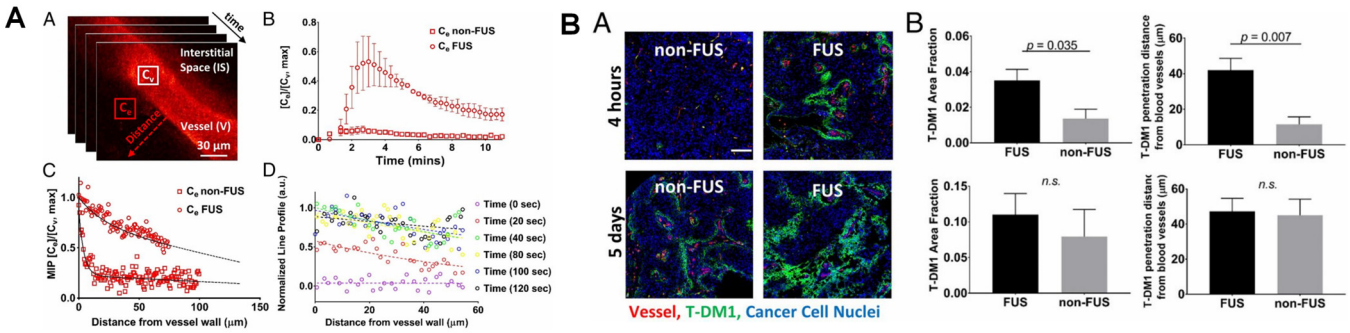

Figure 10. *Cont.*

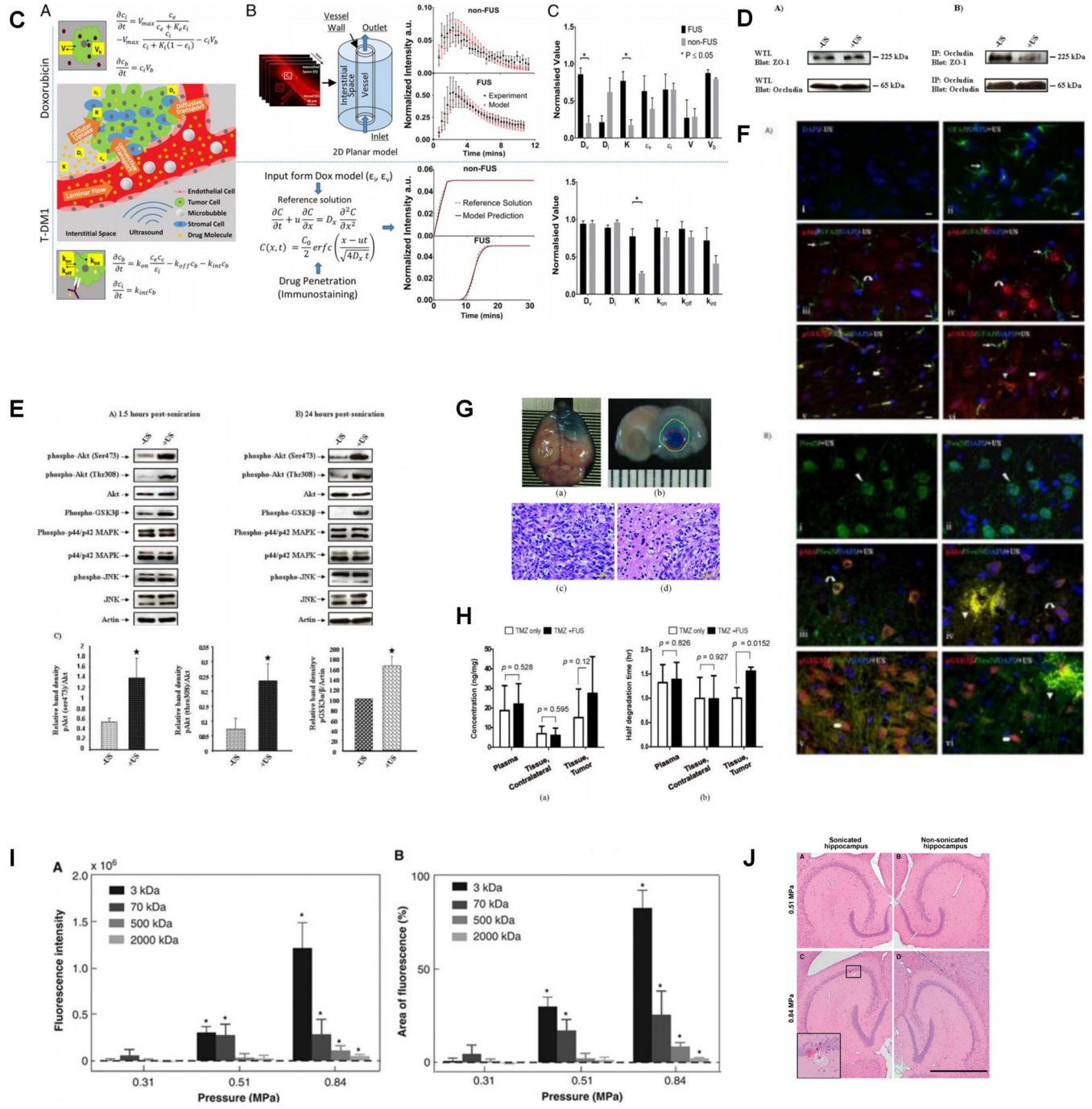

Figure 10. Physical therapies for breaking the safe haven. (**A**) FUS enhances doxorubicin (Dox) penetration and promotes convective transport in BT474-Gluc brain tumors [164]. (a) Sequential intravital multiphoton microscopy of Dox autofluorescence. (b) Temporal evaluation of Dox extravasation with and without FUS-BTB disruption. Cv and Ce are the mean pixel intensity of the vessel and the extravascular space, respectively. The maximum mean fluorescence for the FUS and non-FUS was 0.52 ± 0.15 and 0.07 ± 0.02, a sevenfold difference. (c) Dox penetration from a line profile perpendicular to vessel wall (red dotted arrow in a). The plot shows the normalized maximum intensity projection (MIP) across the series of images. The dotted line shows a regression fitted to the data from four different animals for each condition (non-FUS and FUS). (d) Representative data of the temporal evolution of the normalized intensity of the line profile (red dotted arrow in a). For consistency in the notation of the experiments/modeling, Cv is the Dox intensity/concentration in

the vessel, Ce is the Dox intensity/concentration in the extracellular/interstitial space. (**B**) FUS-BTB disruption increases early extravasation and penetration of T-DM1 in BT474-Gluc brain tumors [164]. (a) Representative microscopy data of TDM1 extravasation with and without FUS at 4 h and 5 d. (b) Quantification of the T-DM1 extravasation (Left) and penetration (Right) with and without FUS at 4 h (Upper) and 5 d (Lower) posttreatment. Parametric Student's t test for $p < 0.05$. (**C**) The quantification of transvascular transport via mathematical modeling demonstrates a multifold increase in the effective diffusion coefficient (4.3-fold) and in hydraulic conductivity (4.5–fold) after FUS-BTB disruption [164]. (a) Schematic illustrating the transport of the anticancer agents from the vessel to the interstitial space along with the studied model parameters and agent-specific cellular uptake model equations. (Upper) Convection–diffusion–reaction model following Michaelis–Menten kinetics with binding of doxorubicin to DNA (Vb). (Lower) Convection–diffusion–reaction model for T-DM1. Excellent fit was observed for both doxorubicin and T-DM1. (b, Upper) The time dependence of doxorubicin extravasation from the fitted and experimental data for non–FUS and FUS–BBB/BTB disruption groups. (b, Lower) Parameter fit methodology for T–DM1 and fitted data from two different experiments. The fitted vascular and interstitial effective porosity (fraction of surface area occupied by pores) from the doxorubicin model was used as input to the T-DM1 fitting (i.e., same animal model). (c) Normalized parameter fit for non-FUS and FUS-BBB/BTB disruption groups (Upper, doxorubicin; Lower, T-DM1). The values for each parameter were normalized to maximum to be displayed on the same plot. The exact numbers and their units are shown in Tables 1 and 2 for doxorubicin and T-DM1, respectively. (**D**) The diminished interaction of intracellular scaffolding proteins ZO-1 and occludin as a result of ultrasound treatment [166]. (a) Western Blot analysis on whole brain tissue lysates (WTL) shows that ZO-1 and occludin protein levels are not changed in response to ultrasound treatment. (b), Co-immunoprecipitation of occludin and ZO-1. The amount of occludin co-precipitating with ZO-1 in the presence of US-treatment is reduced when compared to non-sonicated brains (-US). (**E**) Ultrasound in the presence of microbubbles increases the activity of the Akt signaling pathway, while the activity of MAPK signaling remains unchanged [166]. Brains were removed 1.5 h (a) or 24 h (b) post-sonication and snap-frozen using liquid nitrogen. Brain tissue regions with trypan blue leakage in the sonicated hemisphere (+US) and the equivalent area from opposite hemisphere (-US) were then homogenized with RIPA lysis buffer. Equal amounts of extracted proteins were analyzed by western blotting for the indicated proteins. (c) Graphical representation of three independent experiments illustrating the marked increase in pAkt (Ser473), pAkt (Thre308) and pGSK3b (Ser9) 1.5 hrs after sonication treatment. The star (*) represents $p < 0.05$ for -US versus +US. (**F**) Increased phosphorylation of Akt and GSK3β in neuronal cells of sonicated rat brain regions [166]. (a) Panel [i] shows a control section without application of any primary antibodies. Panel [ii] represents a direct staining of the astrocytes with Alexa-fluor488-conjugated GFAP (green, right arrow). Panels [iii] and [iv] represent immunofluorescence staining with pAkt (red, curved arrow) and GFAP (green, right arrow) in non-sonicated (-US) as well as sonicated (+US) hemispheres respectively. Panels [v] and [vi] illustrate co-staining of pGSK3b (red, pentagon) and GFAP (green, right arrow) in '-US' and '+US' brain regions respectively. (b) Panels [ii] and [iii] represent neuronal cells morphology as directly stained with Alexa-Fluor 488-conjugated NeuN (green, lightning bolt). Co-staining of pAkt (red, curved arrow) with NeuN (green) and also pGSK3b (red, pentagon) with NeuN (green) are shown in panels [iii, iv] and [v, vi] respectively. The regions of the brain sections with IgG extravasation (arrow head) and their surrounding neuronal cells with elevated levels of pAkt and pGSK3b are shown in panels [iv, vi]. (**G**) Representative Evans Blue (EB) dye staining in animal brains after FUS-BBB opening [167]. (**H**) (a) The TMZ concentration (mean ± STD) at 2 h after TMZ administration obtained from plasma and brain tissues from each experimental group. (b) The estimated time (in hours) for TMZ to degrade to 50% of the peak level [167]. (**I**) (a) The average fluorescence intensity and (b) average area of fluorescence for the 3, 70, 500, and 2000 kDa dextrans sonicated at 0.31, 0.51, and 0.84 MPa. The pressure threshold for significant increases in both fluorescence and the area of fluorescence was 0.51 MPa for 3 and 70 kDa dextrans. However, it increased to 0.84 MPa for the 500 and 2000 kDa dextrans [169]. (**J**) Microscopic examination of (a,c) left (sonicated) and (b,d) the corresponding right (nonsonicated) hippocampi in hemotoxylin and eosin-stained, 6 μm-thick horizontal sections [169].

In summary, FUS-assisted BBB anticancer drug therapy has great potential, and after further optimization research, it may promote the development of personalized intracerebral therapy. In addition, radio-frequency microwave and laser interstitial thermotherapy can also induce the destruction of the blood–brain tumor barrier through heating. They use induced DNA damage and laser ablation hyperthermia to destroy brain tumor tissue, respectively, and achieve good results in clinical trials [170,171].

4. Conclusions and Prospectives

Cancer drug resistance presents a multifaceted challenge involving various parameters, each acting as a critical pivot influencing downstream signaling. This phenomenon not only adapts to current drug environments but also explores alternative survival mechanisms. The inherent heterogeneity of tumors, coupled with intratumoral physiological barriers and supportive safe harbors, further complicates the issue. In this paper, we propose that "heterogeneity, intratumoral physiological barriers, and safe harbors serve as the origins, breeding grounds, and natural shelters of drug resistance, respectively". We delineate the roles of these factors in the onset and progression of tumor drug resistance and summarize corresponding strategies, which aim to manage the origins of drug resistance, dismantle its breeding grounds, and disrupt its safe harbors through a "three-step approach".

The first step involves managing cancer evolution and implementing early intervention. Leveraging liquid biopsy sequencing and extensive bioinformatics tools has elucidated patterns of clonal and subclonal mutations linked to tumor resistance. Combining drugs targeting subclonal mutations to prevent convergent evolution, modeling quantitative cloning for adjuvant drug planning, utilizing clonal neoantigen vaccines, and adopting adoptive T-cell therapy will effectively increase clinical benefits and prolong survival.

The next step involves normalizing intratumoral physiological barriers, including the blood–lymphatic network and the extracellular matrix. Modulating internal physiological barrier function to replace the combination of multiple drugs addresses the proliferation of complex tumor multi-drug resistance subtypes, thereby facilitating the delivery and accumulation of multiple drugs in a non-specific manner.

The last step involves disrupting tumor safe havens. Through biochemical and physical methods, efforts are made to breach the blood–brain barrier, enhancing the distribution and concentration of anticancer agents within brain tissue. This strategy effectively extends the survival of patients with brain metastases and primary brain tumors, crucially allowing for extended treatment opportunities and better management of complications.

Through the above "three-step approach", we have established a framework for "dissecting" cancer resistance, which enables the resistance caused by different mechanisms to be tackled as separate working units and then considered in a global way. Combining in-depth analysis of the original drivers of tumor resistance, full consideration of the normalized tumor environment, and finally breaking the safe haven based on tumor escape is undoubtedly a challenging but formative approach to combat cancer resistance to treatment. However, we also realize that even in the research setting, systematic analysis of cancer genetic lineages remains imperfect. Acquiring sufficient high-quality tumor material to pinpoint the dominant influential resistance mechanism among multiple mutations remains a formidable challenge. While predictive modeling can streamline the identification of resistance mutations beforehand, its effectiveness hinges on the training and validation of clinical data. Therefore, to overcome this obstacle, dedicated multidisciplinary teams and patients are required to implement rigorous scholarly efforts in this area.

Furthermore, even after the resistance mechanism is deciphered, the oncology field's capability to evaluate rational drug combinations in clinical trials remains restricted. There is an urgent need to develop more effective drug testing protocols for assessing combination therapy strategies within well-defined molecular contexts. In parallel, enhancing the development of targeted therapies through rational design, such as personalized tumor vaccines and multi-target inhibitors, is crucial. These innovations are essential for advancing the treatment of drug-resistant cancers.

In addition to inhibiting the source, normalizing the tumor microenvironment also enhances drug efficacy. However, significant inter-patient variability necessitates further clinical data to establish the concept of the normalization window. This also emphasizes the importance of clear guidelines to recommend effective treatment doses, times, and durations, while enhancing the function of the vascular–lymphatic network and optimizing the extracellular matrix to minimize side effects.

Finally, advancing comprehensive methods to assess and quantify extravasation across or the disruption of the BBB/BTB remains the foremost priority in breaking the safe havens effectively. While enhanced MRI serves as the gold standard for evaluating BBB function, integrating in vitro data to elucidate interactions between efflux and uptake transporters and drug metabolism could enhance the precision of treatment strategies. Hence, investigating biomarkers and single-cell profiles of vascular neural units during primary brain tumor progression and metastasis is crucial for advancing personalized strategies to break safe havens effectively.

While the comprehensive analysis of the factors contributing to cancer resistance and their underlying mechanisms requires sustained effort over time, the foundational framework of cancer resistance has steadily improved. As multidisciplinary research continues to fill in the knowledge and details within this framework, achieving the goal of curing cancer becomes increasingly attainable.

Author Contributions: S.Z.: literature review, manuscript preparation, and writing—original draft. X.W.: review and editing. H.J.: review and editing. All authors have read and agreed to the published version of the manuscript.

Funding: This work was funded by grants from the National Natural Science Foundation of China (Nos. 21974019, 92061121, 82027806, and 82061148012).

Conflicts of Interest: The authors declare no conflicts of interest.

References

1. Sung, H.; Ferlay, J.; Siegel, R.L.; Laversanne, M.; Soerjomataram, I.; Jemal, A.; Bray, F. Global Cancer Statistics 2020: GLOBOCAN Estimates of Incidence and Mortality Worldwide for 36 Cancers in 185 Countries. *CA A Cancer J. Clin.* **2021**, *71*, 209–249. [CrossRef] [PubMed]
2. Sansregret, L.; Vanhaesebroeck, B.; Swanton, C. Determinants and clinical implications of chromosomal instability in cancer. *Nat. Rev. Clin. Oncol.* **2018**, *15*, 139–150. [CrossRef] [PubMed]
3. Stephens, P.J.; Greenman, C.D.; Fu, B.; Yang, F.; Bignell, G.R.; Mudie, L.J.; Pleasance, E.D.; Lau, K.W.; Beare, D.; Stebbings, L.A.; et al. Massive Genomic Rearrangement Acquired in a Single Catastrophic Event during Cancer Development. *Cell* **2011**, *144*, 27–40. [CrossRef] [PubMed]
4. Greaves, M. Evolutionary determinants of cancer. *Cancer Discov.* **2015**, *5*, 806–820. [CrossRef]
5. Johnson, B.E.; Mazor, T.; Hong, C.; Barnes, M.; Aihara, K.; McLean, C.Y.; Fouse, S.D.; Yamamoto, S.; Ueda, H.; Tatsuno, K.; et al. Mutational Analysis Reveals the Origin and Therapy-Driven Evolution of Recurrent Glioma. *Science* **2014**, *343*, 189–193. [CrossRef]
6. Vo, J.N.; Wu, Y.-M.; Mishler, J.; Hall, S.; Mannan, R.; Wang, L.; Ning, Y.; Zhou, J.; Hopkins, A.C.; Estill, J.C.; et al. The genetic heterogeneity and drug resistance mechanisms of relapsed refractory multiple myeloma. *Nat. Commun.* **2022**, *13*, 3750. [CrossRef]
7. Fischer, E.S.; Böhm, K.; Lydeard, J.R.; Yang, H.; Stadler, M.B.; Cavadini, S.; Nagel, J.; Serluca, F.; Acker, V.; Lingaraju, G.M.; et al. Structure of the DDB1–CRBN E3 ubiquitin ligase in complex with thalidomide. *Nature* **2014**, *512*, 49–53. [CrossRef]
8. Krönke, J.; Udeshi, N.D.; Narla, A.; Grauman, P.; Hurst, S.N.; McConkey, M.; Svinkina, T.; Heckl, D.; Comer, E.; Li, X.; et al. Lenalidomide Causes Selective Degradation of IKZF1 and IKZF3 in Multiple Myeloma Cells. *Science* **2014**, *343*, 301–305. [CrossRef]
9. McGranahan, N.; Swanton, C. Clonal Heterogeneity and Tumor Evolution: Past, Present, and the Future. *Cell* **2017**, *168*, 613–628. [CrossRef] [PubMed]
10. Vasan, N.; Baselga, J.; Hyman, D.M. A view on drug resistance in cancer. *Nature* **2019**, *575*, 299–309. [CrossRef]
11. Kim, H.; Zheng, S.; Amini, S.S.; Virk, S.M.; Mikkelsen, T.; Brat, D.J.; Grimsby, J.; Sougnez, C.; Muller, F.; Hu, J.; et al. Whole-genome and multisector exome sequencing of primary and post-treatment glioblastoma reveals patterns of tumor evolution. *Genome Res.* **2015**, *25*, 316–327. [CrossRef] [PubMed]
12. Coombs, C.C.; Zehir, A.; Devlin, S.M.; Kishtagari, A.; Syed, A.; Jonsson, P.; Hyman, D.M.; Solit, D.B.; Robson, M.E.; Baselga, J.; et al. Therapy-Related Clonal Hematopoiesis in Patients with Non-hematologic Cancers Is Common and Associated with Adverse Clinical Outcomes. *Cell Stem. Cell* **2017**, *21*, 374–382 e4. [CrossRef]

13. Lindsley, R.C.; Saber, W.; Mar, B.G.; Redd, R.; Wang, T.; Haagenson, M.D.; Grauman, P.V.; Hu, Z.-H.; Spellman, S.R.; Lee, S.J.; et al. Prognostic Mutations in Myelodysplastic Syndrome after Stem-Cell Transplantation. *N. Engl. J. Med.* **2017**, *376*, 536–547. [CrossRef] [PubMed]
14. Baish, J.W.; Jain, R.K. Fractals and Cancer1. *Cancer Res.* **2000**, *60*, 3683–3688. [PubMed]
15. Vakoc, B.J.; Lanning, R.M.; Tyrrell, J.A.; Padera, T.P.; Bartlett, L.A.; Stylianopoulos, T.; Munn, L.L.; Tearney, G.J.; Fukumura, D.; Jain, R.K.; et al. Three-dimensional microscopy of the tumor microenvironment in vivo using optical frequency domain imaging. *Nat. Med.* **2009**, *15*, 1219–1223. [CrossRef]
16. Hobbs, S.K.; Monsky, W.L.; Yuan, F.; Roberts, W.G.; Griffith, L.; Torchilin, V.P.; Jain, R.K. Regulation of transport pathways in tumor vessels: Role of tumor type and microenvironment. *Proc. Natl. Acad. Sci. USA* **1998**, *95*, 4607–4612. [CrossRef]
17. Jain, R.K. Transport of molecules across tumor vasculature. *Cancer Metastasis Rev.* **1987**, *6*, 559–593. [CrossRef]
18. Jain, R.K.; Stylianopoulos, T. Delivering nanomedicine to solid tumors. *Nat. Rev. Clin. Oncol.* **2010**, *7*, 653–664. [CrossRef]
19. Endrich, B.; Reinhold, H.S.; Gross, J.F.; Intaglietta, M. Tissue Perfusion Inhomogeneity During Early Tumor Growth in Rats2. *JNCI J. Natl. Cancer Inst.* **1979**, *62*, 387–395. [CrossRef]
20. Sanna, K.; Rofstad, E.K. Hypoxia-induced resistance to doxorubicin and methotrexate in human melanoma cell lines in vitro. *Int. J. Cancer* **1994**, *58*, 258–262. [CrossRef]
21. Jain, R.K. Transport Phenomena in Tumors. In *Advances in Chemical Engineering*; Wei, J., Ed.; Academic Press: Cambridge, MA, USA, 1994; Volume 19, pp. 129–200.
22. Kamoun, W.S.; Chae, S.-S.; Lacorre, D.A.; Tyrrell, J.A.; Mitre, M.; Gillissen, M.A.; Fukumura, D.; Jain, R.K.; Munn, L.L. Simultaneous measurement of RBC velocity, flux, hematocrit and shear rate in vascular networks. *Nat. Methods* **2010**, *7*, 655–660. [CrossRef] [PubMed]
23. Yuan, F.; Dellian, M.; Fukumura, D.; Leunig, M.; Berk, D.A.; Torchilin, V.P.; Jain, R.K. Vascular Permeability in a Human Tumor Xenograft: Molecular Size Dependence and Cutoff Size1. *Cancer Res.* **1995**, *55*, 3752–3756. [PubMed]
24. Yuan, F.; Salehi, H.A.; Boucher, Y.; Vasthare, U.S.; Tuma, R.F.; Jain, R.K. Vascular Permeability and Microcirculation of Gliomas and Mammary Carcinomas Transplanted in Rat and Mouse Cranial Windows1. *Cancer Res.* **1994**, *54*, 4564–4568.
25. Hagendoorn, J.; Tong, R.; Fukumura, D.; Lin, Q.; Lobo, J.; Padera, T.P.; Xu, L.; Kucherlapati, R.; Jain, R.K. Onset of Abnormal Blood and Lymphatic Vessel Function and Interstitial Hypertension in Early Stages of Carcinogenesis. *Cancer Res.* **2006**, *66*, 3360–3364. [CrossRef] [PubMed]
26. Padera, T.P.; Stoll, B.R.; Tooredman, J.B.; Capen, D.; Tomaso, E.D.; Jain, R.K. Cancer cells compress intratumour vessels. *Nature* **2004**, *427*, 695. [CrossRef]
27. Boucher, Y.; Baxter, L.T.; Jain, R.K. Interstitial Pressure Gradients in Tissue-isolated and Subcutaneous Tumors: Implications for Therapy1. *Cancer Res.* **1990**, *50*, 4478–4484.
28. Jain, R.K.; Baxter, L.T. Mechanisms of Heterogeneous Distribution of Monoclonal Antibodies and Other Macromolecules in Tumors: Significance of Elevated Interstitial Pressure1. *Cancer Res.* **1988**, *48*, 7022–7032. [PubMed]
29. Jain, R.K.; Tong, R.T.; Munn, L.L. Effect of Vascular Normalization by Antiangiogenic Therapy on Interstitial Hypertension, Peritumor Edema, and Lymphatic Metastasis: Insights from a Mathematical Model. *Cancer Res.* **2007**, *67*, 2729–2735. [CrossRef]
30. Baxter, L.T.; Jain, R.K. Transport of fluid and macromolecules in tumors. I. Role of interstitial pressure and convection. *Microvasc. Res.* **1989**, *37*, 77–104. [CrossRef]
31. Baxter, L.T.; Jain, R.K. Transport of fluid and macromolecules in tumors. II. Role of heterogeneous perfusion and lymphatics. *Microvasc. Res.* **1990**, *40*, 246–263. [CrossRef]
32. Jain, R.K. Delivery of Novel Therapeutic Agents in Tumors: Physiological Barriers and Strategies. *JNCI J. Natl. Cancer Inst.* **1990**, *81*, 570–576. [CrossRef] [PubMed]
33. Spivak-Kroizman, T.R.; Hostetter, G.; Posner, R.; Aziz, M.; Hu, C.; Demeure, M.J.; Von Hoff, D.; Hingorani, S.R.; Palculict, T.B.; Izzo, J.; et al. Hypoxia Triggers Hedgehog-Mediated Tumor–Stromal Interactions in Pancreatic Cancer. *Cancer Res.* **2013**, *73*, 3235–3247. [CrossRef] [PubMed]
34. Stylianopoulos, T.; Martin, J.D.; Chauhan, V.P.; Jain, S.R.; Diop-Frimpong, B.; Bardeesy, N.; Smith, B.L.; Ferrone, C.R.; Hornicek, F.J.; Boucher, Y.; et al. Causes, consequences, and remedies for growth-induced solid stress in murine and human tumors. *Proc. Natl. Acad. Sci. USA* **2012**, *109*, 15101–15108. [CrossRef]
35. Yamada, K.M.; Collins, J.W.; Cruz Walma, D.A.; Doyle, A.D.; Morales, S.G.; Lu, J.; Matsumoto, K.; Nazari, S.S.; Sekiguchi, R.; Shinsato, Y.; et al. Extracellular matrix dynamics in cell migration, invasion and tissue morphogenesis. *Int. J. Exp. Pathol.* **2019**, *100*, 144–152. [CrossRef]
36. Bissell, M.J.; Hall, H.G.; Parry, G. How does the extracellular matrix direct gene expression? *J. Theor. Biol.* **1982**, *99*, 31–68. [CrossRef]
37. Pearce, O.M.T.; Delaine-Smith, R.M.; Maniati, E.; Nichols, S.; Wang, J.; Böhm, S.; Rajeeve, V.; Ullah, D.; Chakravarty, P.; Jones, R.R.; et al. Deconstruction of a Metastatic Tumor Microenvironment Reveals a Common Matrix Response in Human Cancers. *Cancer Discov.* **2018**, *8*, 304–319. [CrossRef]
38. Thorsson, V.; Gibbs, D.L.; Brown, S.D.; Wolf, D.; Bortone, D.S.; Ou Yang, T.-H.; Porta-Pardo, E.; Gao, G.F.; Plaisier, C.L.; Eddy, J.A.; et al. The Immune Landscape of Cancer. *Immunity* **2018**, *48*, 812–830. [CrossRef]
39. Cox, T.R. The matrix in cancer. *Nat. Rev. Cancer* **2021**, *21*, 217–238. [CrossRef]

40. Amatangelo, M.D.; Bassi, D.E.; Klein-Szanto, A.J.P.; Cukierman, E. Stroma-Derived Three-Dimensional Matrices Are Necessary and Sufficient to Promote Desmoplastic Differentiation of Normal Fibroblasts. *Am. J. Pathol.* **2005**, *167*, 475–488. [CrossRef] [PubMed]
41. Piersma, B.; Hayward, M.-K.; Weaver, V.M. Fibrosis and cancer: A strained relationship. *Biochim. Et Biophys. Acta (BBA) Rev. Cancer* **2020**, *1873*, 188356. [CrossRef]
42. Vitale, D.; Kumar Katakam, S.; Greve, B.; Jang, B.; Oh, E.-S.; Alaniz, L.; Götte, M. Proteoglycans and glycosaminoglycans as regulators of cancer stem cell function and therapeutic resistance. *FEBS J.* **2019**, *286*, 2870–2882. [CrossRef] [PubMed]
43. Pires, A.; Greenshields-Watson, A.; Jones, E.; Smart, K.; Lauder, S.N.; Somerville, M.; Milutinovic, S.; Kendrick, H.; Hindley, J.P.; French, R.; et al. Immune Remodeling of the Extracellular Matrix Drives Loss of Cancer Stem Cells and Tumor Rejection. *Cancer Immunol. Res.* **2020**, *8*, 1520–1531. [CrossRef]
44. Filipe, E.C.; Chitty, J.L.; Cox, T.R. Charting the unexplored extracellular matrix in cancer. *Int. J. Exp. Pathol.* **2018**, *99*, 58–76. [CrossRef] [PubMed]
45. Nam, S.; Hu, K.H.; Butte, M.J.; Chaudhuri, O. Strain-enhanced stress relaxation impacts nonlinear elasticity in collagen gels. *Proc. Natl. Acad. Sci. USA* **2016**, *113*, 5492–5497. [CrossRef]
46. Yue, X.; Nguyen, T.D.; Zellmer, V.; Zhang, S.; Zorlutuna, P. Stromal cell-laden 3D hydrogel microwell arrays as tumor microenvironment model for studying stiffness dependent stromal cell-cancer interactions. *Biomaterials* **2018**, *170*, 37–48. [CrossRef]
47. Tian, C.; Clauser, K.R.; Öhlund, D.; Rickelt, S.; Huang, Y.; Gupta, M.; Mani, D.R.; Carr, S.A.; Tuveson, D.A.; Hynes, R.O. Proteomic analyses of ECM during pancreatic ductal adenocarcinoma progression reveal different contributions by tumor and stromal cells. *Proc. Natl. Acad. Sci. USA* **2019**, *116*, 19609–19618. [CrossRef]
48. Kuninty, P.R.; Bansal, R.; De Geus, S.W.L.; Mardhian, D.F.; Schnittert, J.; van Baarlen, J.; Storm, G.; Bijlsma, M.F.; van Laarhoven, H.W.; Metselaar, J.M.; et al. ITGA5 inhibition in pancreatic stellate cells attenuates desmoplasia and potentiates efficacy of chemotherapy in pancreatic cancer. *Sci. Adv.* **2019**, *5*, eaax2770. [CrossRef]
49. Below, C.R.; Kelly, J.; Brown, A.; Humphries, J.D.; Hutton, C.; Xu, J.; Lee, B.Y.; Cintas, C.; Zhang, X.; Hernandez-Gordillo, V.; et al. A microenvironment-inspired synthetic three-dimensional model for pancreatic ductal adenocarcinoma organoids. *Nat. Mater.* **2022**, *21*, 110–119. [CrossRef] [PubMed]
50. Rice, A.J.; Cortes, E.; Lachowski, D.; Cheung, B.C.H.; Karim, S.A.; Morton, J.P.; del Río Hernández, A. Matrix stiffness induces epithelial–mesenchymal transition and promotes chemoresistance in pancreatic cancer cells. *Oncogenesis* **2017**, *6*, e352. [CrossRef]
51. Hamidi, H.; Ivaska, J. Every step of the way: Integrins in cancer progression and metastasis. *Nat. Rev. Cancer* **2018**, *18*, 533–548. [CrossRef]
52. Yang, X.H.; Flores, L.M.; Li, Q.; Zhou, P.; Xu, F.; Krop, I.E.; Hemler, M.E. Disruption of Laminin-Integrin-CD151-Focal Adhesion Kinase Axis Sensitizes Breast Cancer Cells to ErbB2 Antagonists. *Cancer Res.* **2010**, *70*, 2256–2263. [CrossRef] [PubMed]
53. Pupa, S.M.; Giuffré, S.; Castiglioni, F.; Bertola, L.; Cantú, M.; Bongarzone, I.; Baldassari, P.; Mortarini, R.; Argraves, W.S.; Anichini, A.; et al. Regulation of Breast Cancer Response to Chemotherapy by Fibulin-1. *Cancer Res.* **2007**, *67*, 4271–4277. [CrossRef] [PubMed]
54. Hirata, E.; Girotti, M.R.; Viros, A.; Hooper, S.; Spencer-Dene, B.; Matsuda, M.; Larkin, J.; Marais, R.; Sahai, E. Intravital Imaging Reveals How BRAF Inhibition Generates Drug-Tolerant Microenvironments with High Integrin β1/FAK Signaling. *Cancer Cell* **2015**, *27*, 574–588. [CrossRef] [PubMed]
55. Crawford, Y.; Kasman, I.; Yu, L.; Zhong, C.; Wu, X.; Modrusan, Z.; Kaminker, J.; Ferrara, N. PDGF-C Mediates the Angiogenic and Tumorigenic Properties of Fibroblasts Associated with Tumors Refractory to Anti-VEGF Treatment. *Cancer Cell* **2009**, *15*, 21–34. [CrossRef]
56. O'Brown, N.M.; Pfau, S.J.; Gu, C. Bridging barriers: A comparative look at the blood-brain barrier across organisms. *Genes Dev.* **2018**, *32*, 466–478. [CrossRef]
57. Hendricks, B.K.; Cohen-Gadol, A.A.; Miller, J.C. Novel delivery methods bypassing the blood-brain and blood-tumor barriers. *Neurosurg. Focus FOC* **2015**, *38*, E10. [CrossRef]
58. Abbott, N.J.; Rönnbäck, L.; Hansson, E. Astrocyte–endothelial interactions at the blood–brain barrier. *Nat. Rev. Neurosci.* **2006**, *7*, 41–53. [CrossRef]
59. Giepmans, B.N.G.; van Ijzendoorn, S.C.D. Epithelial cell–cell junctions and plasma membrane domains. *Biochim. Et Biophys. Acta (BBA) Biomembr.* **2009**, *1788*, 820–831. [CrossRef]
60. Agarwal, S.; Sane, R.; Gallardo, J.L.; Ohlfest, J.R.; Elmquist, W.F. Distribution of Gefitinib to the Brain Is Limited by P-glycoprotein (ABCB1) and Breast Cancer Resistance Protein (ABCG2)-Mediated Active Efflux. *J. Pharmacol. Exp. Ther.* **2010**, *334*, 147–155. [CrossRef]
61. Demeule, M.; Régina, A.; Jodoin, J.; Laplante, A.; Dagenais, C.; Berthelet, F.; Moghrabi, A.; Béliveau, R. Drug transport to the brain: Key roles for the efflux pump P-glycoprotein in the blood–brain barrier. *Vasc. Pharmacol.* **2002**, *38*, 339–348. [CrossRef]
62. Wang, D.; Wang, C.; Wang, L.; Chen, Y. A comprehensive review in improving delivery of small-molecule chemotherapeutic agents overcoming the blood-brain/brain tumor barriers for glioblastoma treatment. *Drug Deliv.* **2019**, *26*, 551–565. [CrossRef] [PubMed]
63. Arvanitis, C.D.; Ferraro, G.B.; Jain, R.K. The blood–brain barrier and blood–tumour barrier in brain tumours and metastases. *Nat. Rev. Cancer* **2020**, *20*, 26–41. [CrossRef] [PubMed]

64. Monsky, W.L.; Carreira, C.M.; Tsuzuki, Y.; Gohongi, T.; Fukumura, D.; Jain, R.K. Role of Host Microenvironment in Angiogenesis and Microvascular Functions in Human Breast Cancer Xenografts: Mammary Fat Pad versus Cranial Tumors1. *Clin. Cancer Res.* **2002**, *8*, 1008–1013. [PubMed]
65. Pitz, M.W.; Desai, A.; Grossman, S.A.; Blakeley, J.O. Tissue concentration of systemically administered antineoplastic agents in human brain tumors. *J. Neuro-Oncol.* **2011**, *104*, 629–638. [CrossRef] [PubMed]
66. Deeken, J.F.; Löscher, W. The Blood-Brain Barrier and Cancer: Transporters, Treatment, and Trojan Horses. *Clin. Cancer Res.* **2007**, *13*, 1663–1674. [CrossRef]
67. Sarkaria, J.N.; Hu, L.S.; Parney, I.F.; Pafundi, D.H.; Brinkmann, D.H.; Laack, N.N.; Giannini, C.; Burns, T.C.; Kizilbash, S.H.; Laramy, J.K.; et al. Is the blood–brain barrier really disrupted in all glioblastomas? A critical assessment of existing clinical data. *Neuro-Oncology* **2017**, *20*, 184–191. [CrossRef]
68. Gerlinger, M.; Rowan, A.J.; Horswell, S.; Larkin, J.; Endesfelder, D.; Gronroos, E.; Martinez, P.; Matthews, N.; Stewart, A.; Tarpey, P.; et al. Intratumor Heterogeneity and Branched Evolution Revealed by Multiregion Sequencing. *N. Engl. J. Med.* **2012**, *366*, 883–892. [CrossRef] [PubMed]
69. Ha, G.; Roth, A.; Khattra, J.; Ho, J.; Yap, D.; Prentice, L.M.; Melnyk, N.; McPherson, A.; Bashashati, A.; Laks, E.; et al. TITAN: Inference of copy number architectures in clonal cell populations from tumor whole-genome sequence data. *Genome Res.* **2014**, *24*, 1881–1893. [CrossRef]
70. Roth, A.; Khattra, J.; Yap, D.; Wan, A.; Laks, E.; Biele, J.; Ha, G.; Aparicio, S.; Bouchard-Côté, A.; Shah, S.P. PyClone: Statistical inference of clonal population structure in cancer. *Nat. Methods* **2014**, *11*, 396–398. [CrossRef]
71. Van Loo, P.; Nordgard, S.H.; Lingjærde, O.C.; Russnes, H.G.; Rye, I.H.; Sun, W.; Weigman, V.J.; Marynen, P.; Zetterberg, A.; Naume, B.; et al. Allele-specific copy number analysis of tumors. *Proc. Natl. Acad. Sci. USA* **2010**, *107*, 16910–16915. [CrossRef]
72. Haber, D.A.; Velculescu, V.E. Blood-Based Analyses of Cancer: Circulating Tumor Cells and Circulating Tumor DNA. *Cancer Discov.* **2014**, *4*, 650–661. [CrossRef] [PubMed]
73. Kotani, D.; Oki, E.; Nakamura, Y.; Yukami, H.; Mishima, S.; Bando, H.; Shirasu, H.; Yamazaki, K.; Watanabe, J.; Kotaka, M.; et al. Molecular residual disease and efficacy of adjuvant chemotherapy in patients with colorectal cancer. *Nat. Med.* **2023**, *29*, 127–134. [CrossRef] [PubMed]
74. Misale, S.; Arena, S.; Lamba, S.; Siravegna, G.; Lallo, A.; Hobor, S.; Russo, M.; Buscarino, M.; Lazzari, L.; Sartore-Bianchi, A.; et al. Blockade of EGFR and MEK Intercepts Heterogeneous Mechanisms of Acquired Resistance to Anti-EGFR Therapies in Colorectal Cancer. *Sci. Transl. Med.* **2014**, *6*, 224ra226. [CrossRef]
75. Bozic, I.; Nowak, M.A. Timing and heterogeneity of mutations associated with drug resistance in metastatic cancers. *Proc. Natl. Acad. Sci. USA* **2014**, *111*, 15964–15968. [CrossRef]
76. Palmer, C.D.; Rappaport, A.R.; Davis, M.J.; Hart, M.G.; Scallan, C.D.; Hong, S.-J.; Gitlin, L.; Kraemer, L.D.; Kounlavouth, S.; Yang, A.; et al. Individualized, heterologous chimpanzee adenovirus and self-amplifying mRNA neoantigen vaccine for advanced metastatic solid tumors: Phase 1 trial interim results. *Nat. Med.* **2022**, *28*, 1619–1629. [CrossRef]
77. Rappaport, A.R.; Kyi, C.; Lane, M.; Hart, M.G.; Johnson, M.L.; Henick, B.S.; Liao, C.-Y.; Mahipal, A.; Shergill, A.; Spira, A.I.; et al. A shared neoantigen vaccine combined with immune checkpoint blockade for advanced metastatic solid tumors: Phase 1 trial interim results. *Nat. Med.* **2024**, *30*, 1013–1022. [CrossRef]
78. Tirosh, I.; Izar, B.; Prakadan, S.M.; Wadsworth, M.H.; Treacy, D.; Trombetta, J.J.; Rotem, A.; Rodman, C.; Lian, C.; Murphy, G.; et al. Dissecting the multicellular ecosystem of metastatic melanoma by single-cell RNA-seq. *Science* **2016**, *352*, 189–196. [CrossRef] [PubMed]
79. Crowley, E.; Di Nicolantonio, F.; Loupakis, F.; Bardelli, A. Liquid biopsy: Monitoring cancer-genetics in the blood. *Nat. Rev. Clin. Oncol.* **2013**, *10*, 472–484. [CrossRef]
80. Wagle, N.; Emery, C.; Berger, M.F.; Davis, M.J.; Sawyer, A.; Pochanard, P.; Kehoe, S.M.; Johannessen, C.M.; MacConaill, L.E.; Hahn, W.C.; et al. Dissecting Therapeutic Resistance to RAF Inhibition in Melanoma by Tumor Genomic Profiling. *J. Clin. Oncol.* **2011**, *29*, 3085–3096. [CrossRef]
81. Gorre, M.E.; Mohammed, M.; Ellwood, K.; Hsu, N.; Paquette, R.; Rao, P.N.; Sawyers, C.L. Clinical Resistance to STI-571 Cancer Therapy Caused by BCR-ABL Gene Mutation or Amplification. *Science* **2001**, *293*, 876–880. [CrossRef]
82. Diaz, L.A., Jr.; Williams, R.T.; Wu, J.; Kinde, I.; Hecht, J.R.; Berlin, J.; Allen, B.; Bozic, I.; Reiter, J.G.; Nowak, M.A.; et al. The molecular evolution of acquired resistance to targeted EGFR blockade in colorectal cancers. *Nature* **2012**, *486*, 537–540. [CrossRef] [PubMed]
83. Misale, S.; Yaeger, R.; Hobor, S.; Scala, E.; Janakiraman, M.; Liska, D.; Valtorta, E.; Schiavo, R.; Buscarino, M.; Siravegna, G.; et al. Emergence of KRAS mutations and acquired resistance to anti-EGFR therapy in colorectal cancer. *Nature* **2012**, *486*, 532–536. [CrossRef] [PubMed]
84. Sequist, L.V.; Waltman, B.A.; Dias-Santagata, D.; Digumarthy, S.; Turke, A.B.; Fidias, P.; Bergethon, K.; Shaw, A.T.; Gettinger, S.; Cosper, A.K.; et al. Genotypic and Histological Evolution of Lung Cancers Acquiring Resistance to EGFR Inhibitors. *Sci. Transl. Med.* **2011**, *3*, 75ra26. [CrossRef] [PubMed]
85. Nazarian, R.; Shi, H.; Wang, Q.; Kong, X.; Koya, R.C.; Lee, H.; Chen, Z.; Lee, M.-K.; Attar, N.; Sazegar, H.; et al. Melanomas acquire resistance to B-RAF(V600E) inhibition by RTK or N-RAS upregulation. *Nature* **2010**, *468*, 973–977. [CrossRef]
86. Choi, Y.L.; Soda, M.; Yamashita, Y.; Ueno, T.; Takashima, J.; Nakajima, T.; Yatabe, Y.; Takeuchi, K.; Hamada, T.; Haruta, H.; et al. EML4-ALK Mutations in Lung Cancer That Confer Resistance to ALK Inhibitors. *N. Engl. J. Med.* **2010**, *363*, 1734–1739. [CrossRef]

87. Yun, C.-H.; Mengwasser, K.E.; Toms, A.V.; Woo, M.S.; Greulich, H.; Wong, K.-K.; Meyerson, M.; Eck, M.J. The T790M mutation in EGFR kinase causes drug resistance by increasing the affinity for ATP. *Proc. Natl. Acad. Sci. USA* **2008**, *105*, 2070–2075. [CrossRef]
88. Luo, L.; Parrish, C.A.; Nevins, N.; McNulty, D.E.; Chaudhari, A.M.; Carson, J.D.; Sudakin, V.; Shaw, A.N.; Lehr, R.; Zhao, H.; et al. ATP-competitive inhibitors of the mitotic kinesin KSP that function via an allosteric mechanism. *Nat. Chem. Biol.* **2007**, *3*, 722–726. [CrossRef]
89. Diehl, F.; Schmidt, K.; Choti, M.A.; Romans, K.; Goodman, S.; Li, M.; Thornton, K.; Agrawal, N.; Sokoll, L.; Szabo, S.A.; et al. Circulating mutant DNA to assess tumor dynamics. *Nat. Med.* **2008**, *14*, 985–990. [CrossRef]
90. Frattini, M.; Gallino, G.; Signoroni, S.; Balestra, D.; Lusa, L.; Battaglia, L.; Sozzi, G.; Bertario, L.; Leo, E.; Pilotti, S.; et al. Quantitative and qualitative characterization of plasma DNA identifies primary and recurrent colorectal cancer. *Cancer Lett.* **2008**, *263*, 170–181. [CrossRef]
91. Leary, R.J.; Sausen, M.; Kinde, I.; Papadopoulos, N.; Carpten, J.D.; Craig, D.; O'Shaughnessy, J.; Kinzler, K.W.; Parmigiani, G.; Vogelstein, B.; et al. Detection of Chromosomal Alterations in the Circulation of Cancer Patients with Whole-Genome Sequencing. *Sci. Transl. Med.* **2012**, *4*, 162ra154. [CrossRef]
92. Forshew, T.; Murtaza, M.; Parkinson, C.; Gale, D.; Tsui, D.W.Y.; Kaper, F.; Dawson, S.-J.; Piskorz, A.M.; Jimenez-Linan, M.; Bentley, D.; et al. Noninvasive Identification and Monitoring of Cancer Mutations by Targeted Deep Sequencing of Plasma DNA. *Sci. Transl. Med.* **2012**, *4*, 136ra168. [CrossRef] [PubMed]
93. Kuhlmann, J.D.; Schwarzenbach, H.; Wimberger, P.; Poetsch, M.; Kimmig, R.; Kasimir-Bauer, S. LOH at 6q and 10q in fractionated circulating DNA of ovarian cancer patients is predictive for tumor cell spread and overall survival. *BMC Cancer* **2012**, *12*, 325. [CrossRef] [PubMed]
94. Chan, K.A.; Jiang, P.; Zheng, Y.W.; Liao, G.J.; Sun, H.; Wong, J.; Siu, S.S.N.; Chan, W.C.; Chan, S.L.; Chan, A.T.; et al. Cancer Genome Scanning in Plasma: Detection of Tumor-Associated Copy Number Aberrations, Single-Nucleotide Variants, and Tumoral Heterogeneity by Massively Parallel Sequencing. *Clin. Chem.* **2013**, *59*, 211–224. [CrossRef] [PubMed]
95. Nygaard, A.D.; Garm Spindler, K.-L.; Pallisgaard, N.; Andersen, R.F.; Jakobsen, A. The prognostic value of KRAS mutated plasma DNA in advanced non-small cell lung cancer. *Lung Cancer* **2013**, *79*, 312–317. [CrossRef]
96. Santarpia, L.; Qi, Y.; Stemke-Hale, K.; Wang, B.; Young, E.J.; Booser, D.J.; Holmes, F.A.; O'Shaughnessy, J.; Hellerstedt, B.; Pippen, J.; et al. Mutation profiling identifies numerous rare drug targets and distinct mutation patterns in different clinical subtypes of breast cancers. *Breast Cancer Res. Treat.* **2012**, *134*, 333–343. [CrossRef]
97. Dawson, S.-J.; Tsui, D.W.Y.; Murtaza, M.; Biggs, H.; Rueda, O.M.; Chin, S.-F.; Dunning, M.J.; Gale, D.; Forshew, T.; Mahler-Araujo, B.; et al. Analysis of Circulating Tumor DNA to Monitor Metastatic Breast Cancer. *N. Engl. J. Med.* **2013**, *368*, 1199–1209. [CrossRef]
98. Higgins, M.J.; Jelovac, D.; Barnathan, E.; Blair, B.; Slater, S.; Powers, P.; Zorzi, J.; Jeter, S.C.; Oliver, G.R.; Fetting, J.; et al. Detection of Tumor PIK3CA Status in Metastatic Breast Cancer Using Peripheral Blood. *Clin. Cancer Res.* **2012**, *18*, 3462–3469. [CrossRef]
99. Murtaza, M.; Dawson, S.-J.; Tsui, D.W.Y.; Gale, D.; Forshew, T.; Piskorz, A.M.; Parkinson, C.; Chin, S.-F.; Kingsbury, Z.; Wong, A.S.C.; et al. Non-invasive analysis of acquired resistance to cancer therapy by sequencing of plasma DNA. *Nature* **2013**, *497*, 108–112. [CrossRef] [PubMed]
100. Isakoff, S.J.; Engelman, J.A.; Irie, H.Y.; Luo, J.; Brachmann, S.M.; Pearline, R.V.; Cantley, L.C.; Brugge, J.S. Breast Cancer–Associated PIK3CA Mutations Are Oncogenic in Mammary Epithelial Cells. *Cancer Res.* **2005**, *65*, 10992–11000. [CrossRef]
101. Kitai, H.; Choi, P.H.; Yang, Y.C.; Boyer, J.A.; Whaley, A.; Pancholi, P.; Thant, C.; Reiter, J.; Chen, K.; Markov, V.; et al. Combined inhibition of KRASG12C and mTORC1 kinase is synergistic in non-small cell lung cancer. *Nat. Commun.* **2024**, *15*, 6076. [CrossRef]
102. Shi, H.; Moriceau, G.; Kong, X.; Lee, M.-K.; Lee, H.; Koya, R.C.; Ng, C.; Chodon, T.; Scolyer, R.A.; Dahlman, K.B.; et al. Melanoma whole-exome sequencing identifies V600EB-RAF amplification-mediated acquired B-RAF inhibitor resistance. *Nat. Commun.* **2012**, *3*, 724. [CrossRef] [PubMed]
103. Kantarjian, H.M.; Larson, R.A.; Guilhot, F.; O'Brien, S.G.; Mone, M.; Rudoltz, M.; Krahnke, T.; Cortes, J.; Druker, B.J.; International Randomized Study of Interferon and STI571 (IRIS) Investigators. Efficacy of imatinib dose escalation in patients with chronic myeloid leukemia in chronic phase. *Cancer* **2009**, *115*, 551–560. [CrossRef] [PubMed]
104. Kantarjian, H.; Pasquini, R.; Lévy, V.; Jootar, S.; Holowiecki, J.; Hamerschlak, N.; Hughes, T.; Bleickardt, E.; Dejardin, D.; Cortes, J.; et al. Dasatinib or high-dose imatinib for chronic-phase chronic myeloid leukemia resistant to imatinib at a dose of 400 to 600 milligrams daily. *Cancer* **2009**, *115*, 4136–4147. [CrossRef] [PubMed]
105. Kobayashi, S.; Boggon, T.J.; Dayaram, T.; Jänne, P.A.; Kocher, O.; Meyerson, M.; Johnson, B.E.; Eck, M.J.; Tenen, D.G.; Halmos, B. *EGFR* Mutation and Resistance of Non–Small-Cell Lung Cancer to Gefitinib. *N. Engl. J. Med.* **2005**, *352*, 786–792. [CrossRef]
106. Shah, N.P.; Nicoll, J.M.; Nagar, B.; Gorre, M.E.; Paquette, R.L.; Kuriyan, J.; Sawyers, C.L. Multiple BCR-ABL kinase domain mutations confer polyclonal resistance to the tyrosine kinase inhibitor imatinib (STI571) in chronic phase and blast crisis chronic myeloid leukemia. *Cancer Cell* **2002**, *2*, 117–125. [CrossRef]
107. Ogino, A.; Kitao, H.; Hirano, S.; Uchida, A.; Ishiai, M.; Kozuki, T.; Takigawa, N.; Takata, M.; Kiura, K.; Tanimoto, M. Emergence of Epidermal Growth Factor Receptor T790M Mutation during Chronic Exposure to Gefitinib in a Non–Small Cell Lung Cancer Cell Line. *Cancer Res.* **2007**, *67*, 7807–7814. [CrossRef]
108. Deininger, M.; Buchdunger, E.; Druker, B.J. The development of imatinib as a therapeutic agent for chronic myeloid leukemia. *Blood* **2005**, *105*, 2640–2653. [CrossRef]
109. Linardou, H.; Dahabreh, I.J.; Bafaloukos, D.; Kosmidis, P.; Murray, S. Somatic EGFR mutations and efficacy of tyrosine kinase inhibitors in NSCLC. *Nat. Rev. Clin. Oncol.* **2009**, *6*, 352–366. [CrossRef]

110. Carter, T.A.; Wodicka, L.M.; Shah, N.P.; Velasco, A.M.; Fabian, M.A.; Treiber, D.K.; Milanov, Z.V.; Atteridge, C.E.; Biggs, W.H.; Edeen, P.T.; et al. Inhibition of drug-resistant mutants of ABL, KIT, and EGF receptor kinases. *Proc. Natl. Acad. Sci. USA* **2005**, *102*, 11011–11016. [CrossRef]
111. Bozic, I.; Reiter, J.G.; Allen, B.; Antal, T.; Chatterjee, K.; Shah, P.; Moon, Y.S.; Yaqubie, A.; Kelly, N.; Le, D.T.; et al. Evolutionary dynamics of cancer in response to targeted combination therapy. *eLife* **2013**, *2*, e00747. [CrossRef]
112. Komarova, N.L.; Katouli, A.A.; Wodarz, D. Combination of Two but Not Three Current Targeted Drugs Can Improve Therapy of Chronic Myeloid Leukemia. *PLoS ONE* **2009**, *4*, e4423. [CrossRef] [PubMed]
113. Katouli, A.A.; Komarova, N.L. The Worst Drug Rule Revisited: Mathematical Modeling of Cyclic Cancer Treatments. *Bull. Math. Biol.* **2011**, *73*, 549–584. [CrossRef] [PubMed]
114. McGranahan, N.; Furness, A.J.S.; Rosenthal, R.; Ramskov, S.; Lyngaa, R.; Saini, S.K.; Jamal-Hanjani, M.; Wilson, G.A.; Birkbak, N.J.; Hiley, C.T.; et al. Clonal neoantigens elicit T cell immunoreactivity and sensitivity to immune checkpoint blockade. *Science* **2016**, *351*, 1463–1469. [CrossRef] [PubMed]
115. Folkman, J. Successful Treatment of an Angiogenic Disease. *N. Engl. J. Med.* **1989**, *320*, 1211–1212. [CrossRef]
116. Boehm, T.; Folkman, J.; Browder, T.; O'Reilly, M.S. Antiangiogenic therapy of experimental cancer does not induce acquired drug resistance. *Nature* **1997**, *390*, 404–407. [CrossRef]
117. Jain, R.K. Normalizing tumor vasculature with anti-angiogenic therapy: A new paradigm for combination therapy. *Nat. Med.* **2001**, *7*, 987–989. [CrossRef]
118. Leung, D.W.; Cachianes, G.; Kuang, W.-J.; Goeddel, D.V.; Ferrara, N. Vascular Endothelial Growth Factor Is a Secreted Angiogenic Mitogen. *Science* **1989**, *246*, 1306–1309. [CrossRef]
119. Kerr, D.J. Targeting angiogenesis in cancer: Clinical development of bevacizumab. *Nat. Clin. Pract. Oncol.* **2004**, *1*, 39–43. [CrossRef]
120. Jones, L.H. Medicinal Chemical Biology. In *Burger's Medicinal Chemistry and Drug Discovery*; John Wiley & Sons, Inc.: Hoboken, NJ, USA, 2021; pp. 1–37. [CrossRef]
121. Miller, K.; Wang, M.; Gralow, J.; Dickler, M.; Cobleigh, M.; Perez, E.A.; Shenkier, T.; Cella, D.; Davidson, N.E. Paclitaxel plus Bevacizumab versus Paclitaxel Alone for Metastatic Breast Cancer. *N. Engl. J. Med.* **2007**, *357*, 2666–2676. [CrossRef]
122. Reck, M.; Pawel, J.V.; Zatloukal, P.; Ramlau, R.; Gorbounova, V.; Hirsh, V.; Leighl, N.; Mezger, J.; Archer, V.; Moore, N.; et al. Phase III Trial of Cisplatin Plus Gemcitabine with Either Placebo or Bevacizumab as First-Line Therapy for Nonsquamous Non–Small-Cell Lung Cancer: AVAiL. *J. Clin. Oncol.* **2009**, *27*, 1227–1234. [CrossRef]
123. Tolaney, S.M.; Boucher, Y.; Duda, D.G.; Martin, J.D.; Seano, G.; Ancukiewicz, M.; Barry, W.T.; Goel, S.; Lahdenrata, J.; Isakoff, S.J.; et al. Role of vascular density and normalization in response to neoadjuvant bevacizumab and chemotherapy in breast cancer patients. *Proc. Natl. Acad. Sci. USA* **2015**, *112*, 14325–14330. [CrossRef] [PubMed]
124. Winkler, F.; Kozin, S.V.; Tong, R.T.; Chae, S.-S.; Booth, M.F.; Garkavtsev, I.; Xu, L.; Hicklin, D.J.; Fukumura, D.; di Tomaso, E.; et al. Kinetics of vascular normalization by VEGFR2 blockade governs brain tumor response to radiation: Role of oxygenation, angiopoietin-1, and matrix metalloproteinases. *Cancer Cell* **2004**, *6*, 553–563. [CrossRef]
125. Tong, R.T.; Boucher, Y.; Kozin, S.V.; Winkler, F.; Hicklin, D.J.; Jain, R.K. Vascular Normalization by Vascular Endothelial Growth Factor Receptor 2 Blockade Induces a Pressure Gradient across the Vasculature and Improves Drug Penetration in Tumors. *Cancer Res.* **2004**, *64*, 3731–3736. [CrossRef] [PubMed]
126. Zhou, Q.; Gallo, J.M. Differential effect of sunitinib on the distribution of temozolomide in an orthotopic glioma model. *Neuro-Oncology* **2009**, *11*, 301–310. [CrossRef]
127. Zhou, Q.; Guo, P.; Gallo, J.M. Impact of Angiogenesis Inhibition by Sunitinib on Tumor Distribution of Temozolomide. *Clin. Cancer Res.* **2008**, *14*, 1540–1549. [CrossRef]
128. Jayson, G.C.; Kerbel, R.; Ellis, L.M.; Harris, A.L. Antiangiogenic therapy in oncology: Current status and future directions. *Lancet* **2016**, *388*, 518–529. [CrossRef] [PubMed]
129. Xian, X.; Hakansson, J.; Stahlberg, A.; Lindblom, P.; Betsholtz, C.; Gerhardt, H.; Semb, H. Pericytes limit tumor cell metastasis. *J. Clin. Investig.* **2006**, *116*, 642–651. [CrossRef]
130. Nasarre, P.; Thomas, M.; Kruse, K.; Helfrich, I.; Wolter, V.; Deppermann, C.; Schadendorf, D.; Thurston, G.; Fiedler, U.; Augustin, H.G. Host-Derived Angiopoietin-2 Affects Early Stages of Tumor Development and Vessel Maturation but Is Dispensable for Later Stages of Tumor Growth. *Cancer Res.* **2009**, *69*, 1324–1333. [CrossRef]
131. Roos-Mattila, M.; Kaprio, T.; Mustonen, H.; Hagström, J.; Saharinen, P.; Haglund, C.; Seppänen, H. The possible dual role of Ang-2 in the prognosis of pancreatic cancer. *Sci. Rep.* **2023**, *13*, 18725. [CrossRef]
132. Holopainen, T.; Saharinen, P.; D'Amico, G.; Lampinen, A.; Eklund, L.; Sormunen, R.; Anisimov, A.; Zarkada, G.; Lohela, M.; Heloterä, H.; et al. Effects of Angiopoietin-2-Blocking Antibody on Endothelial Cell–Cell Junctions and Lung Metastasis. *JNCI J. Natl. Cancer Inst.* **2012**, *104*, 461–475. [CrossRef]
133. Monk, B.J.; Poveda, A.; Vergote, I.; Raspagliesi, F.; Fujiwara, K.; Bae, D.-S.; Oaknin, A.; Ray-Coquard, I.; Provencher, D.M.; Karlan, B.Y.; et al. Final results of a phase 3 study of trebananib plus weekly paclitaxel in recurrent ovarian cancer (TRINOVA-1): Long-term survival, impact of ascites, and progression-free survival-2. *Gynecol. Oncol.* **2016**, *143*, 27–34. [CrossRef] [PubMed]
134. Goel, S.; Gupta, N.; Walcott, B.P.; Snuderl, M.; Kesler, C.T.; Kirkpatrick, N.D.; Heishi, T.; Huang, Y.; Martin, J.D.; Ager, E.; et al. Effects of Vascular-Endothelial Protein Tyrosine Phosphatase Inhibition on Breast Cancer Vasculature and Metastatic Progression. *JNCI J. Natl. Cancer Inst.* **2013**, *105*, 1188–1201. [CrossRef]

135. Chakroborty, D.; Sarkar, C.; Yu, H.; Wang, J.; Liu, Z.; Dasgupta, P.S.; Basu, S. Dopamine stabilizes tumor blood vessels by up-regulating angiopoietin 1 expression in pericytes and Krüppel-like factor-2 expression in tumor endothelial cells. *Proc. Natl. Acad. Sci. USA* **2011**, *108*, 20730–20735. [CrossRef] [PubMed]
136. Maharjan, S.; Kim, K.; Agrawal, V.; Choi, H.-J.; Kim, N.-J.; Kim, Y.-M.; Suh, Y.-G.; Kwon, Y.-G. Sac-1004, a novel vascular leakage blocker, enhances endothelial barrier through the cAMP/Rac/cortactin pathway. *Biochem. Biophys. Res. Commun.* **2013**, *435*, 420–427. [CrossRef]
137. Agrawal, V.; Maharjan, S.; Kim, K.; Kim, N.J.; Son, J.; Lee, K.; Choi, H.J.; Rho, S.S.; Ahn, S.; Won, M.H.; et al. Direct endothelial junction restoration results in significant tumor vascular normalization and metastasis inhibition in mice. *Oncotarget* **2014**, *5*, 2761–2777. [CrossRef]
138. Griffon-Etienne, G.E.; Boucher, Y.; Brekken, C.; Suit, H.D.; Jain, R.K. Taxane-induced Apoptosis Decompresses Blood Vessels and Lowers Interstitial Fluid Pressure in Solid Tumors: Clinical Implications1. *Cancer Res.* **1999**, *59*, 3776–3782. [PubMed]
139. He, Y.; Kozaki, K.-i.; Karpanen, T.; Koshikawa, K.; Yla-Herttuala, S.; Takahashi, T.; Alitalo, K. Suppression of Tumor Lymphangiogenesis and Lymph Node Metastasis by Blocking Vascular Endothelial Growth Factor Receptor 3 Signaling. *JNCI J. Natl. Cancer Inst.* **2002**, *94*, 819–825. [CrossRef]
140. Krishnan, J.; Kirkin, V.; Steffen, A.; Hegen, M.; Weih, D.; Tomarev, S.; Wilting, J.R.; Sleeman, J.P. Differential in Vivo and in Vitro Expression of Vascular Endothelial Growth Factor (VEGF)-C and VEGF-D in Tumors and Its Relationship to Lymphatic Metastasis in Immunocompetent Rats1. *Cancer Res.* **2003**, *63*, 713–722.
141. Laakkonen, P.; Waltari, M.; Holopainen, T.; Takahashi, T.; Pytowski, B.; Steiner, P.; Hicklin, D.; Persaud, K.; Tonra, J.R.; Witte, L.; et al. Vascular Endothelial Growth Factor Receptor 3 Is Involved in Tumor Angiogenesis and Growth. *Cancer Res.* **2007**, *67*, 593–599. [CrossRef]
142. Roberts, N.; Kloos, B.; Cassella, M.; Podgrabinska, S.; Persaud, K.; Wu, Y.; Pytowski, B.; Skobe, M. Inhibition of VEGFR-3 Activation with the Antagonistic Antibody More Potently Suppresses Lymph Node and Distant Metastases than Inactivation of VEGFR-2. *Cancer Res.* **2006**, *66*, 2650–2657. [CrossRef]
143. Shimizu, K.; Kubo, H.; Yamaguchi, K.; Kawashima, K.; Ueda, Y.; Matsuo, K.; Awane, M.; Shimahara, Y.; Takabayashi, A.; Yamaoka, Y.; et al. Suppression of VEGFR-3 signaling inhibits lymph node metastasis in gastric cancer. *Cancer Sci.* **2004**, *95*, 328–333. [CrossRef] [PubMed]
144. Fankhauser, M.; Broggi, M.A.S.; Potin, L.; Bordry, N.; Jeanbart, L.; Lund, A.W.; Da Costa, E.; Hauert, S.; Rincon-Restrepo, M.; Tremblay, C.; et al. Tumor lymphangiogenesis promotes T cell infiltration and potentiates immunotherapy in melanoma. *Sci. Transl. Med.* **2017**, *9*, eaal4712. [CrossRef] [PubMed]
145. Hu, X.; Deng, Q.; Ma, L.; Li, Q.; Chen, Y.; Liao, Y.; Zhou, F.; Zhang, C.; Shao, L.; Feng, J.; et al. Meningeal lymphatic vessels regulate brain tumor drainage and immunity. *Cell Res.* **2020**, *30*, 229–243. [CrossRef]
146. Song, E.; Mao, T.; Dong, H.; Boisserand, L.S.B.; Antila, S.; Bosenberg, M.; Alitalo, K.; Thomas, J.-L.; Iwasaki, A. VEGF-C-driven lymphatic drainage enables immunosurveillance of brain tumours. *Nature* **2020**, *577*, 689–694. [CrossRef]
147. McKee, T.D.; Grandi, P.; Mok, W.; Alexandrakis, G.; Insin, N.; Zimmer, J.P.; Bawendi, M.G.; Boucher, Y.; Breakefield, X.O.; Jain, R.K. Degradation of Fibrillar Collagen in a Human Melanoma Xenograft Improves the Efficacy of an Oncolytic Herpes Simplex Virus Vector. *Cancer Res.* **2006**, *66*, 2509–2513. [CrossRef]
148. Mok, W.; Boucher, Y.; Jain, R.K. Matrix Metalloproteinases-1 and -8 Improve the Distribution and Efficacy of an Oncolytic Virus. *Cancer Res.* **2007**, *67*, 10664–10668. [CrossRef]
149. Perentes, J.Y.; McKee, T.D.; Ley, C.D.; Mathiew, H.; Dawson, M.; Padera, T.P.; Munn, L.L.; Jain, R.K.; Boucher, Y. In vivo imaging of extracellular matrix remodeling by tumor-associated fibroblasts. *Nat. Methods* **2009**, *6*, 143–145. [CrossRef] [PubMed]
150. Nakai, Y.; Isayama, H.; Ijichi, H.; Sasaki, T.; Sasahira, N.; Hirano, K.; Kogure, H.; Kawakubo, K.; Yagioka, H.; Yashima, Y.; et al. Inhibition of renin–angiotensin system affects prognosis of advanced pancreatic cancer receiving gemcitabine. *Br. J. Cancer* **2010**, *103*, 1644–1648. [CrossRef]
151. Wilop, S.; von Hobe, S.; Crysandt, M.; Esser, A.; Osieka, R.; Jost, E. Impact of angiotensin I converting enzyme inhibitors and angiotensin II type 1 receptor blockers on survival in patients with advanced non-small-cell lung cancer undergoing first-line platinum-based chemotherapy. *J. Cancer Res. Clin. Oncol.* **2009**, *135*, 1429–1435. [CrossRef]
152. Keizman, D.; Huang, P.; Eisenberger, M.A.; Pili, R.; Kim, J.J.; Antonarakis, E.S.; Hammers, H.; Carducci, M.A. Angiotensin system inhibitors and outcome of sunitinib treatment in patients with metastatic renal cell carcinoma: A retrospective examination. *Eur. J. Cancer* **2011**, *47*, 1955–1961. [CrossRef]
153. Liu, J.; Liao, S.; Diop-Frimpong, B.; Chen, W.; Goel, S.; Naxerova, K.; Ancukiewicz, M.; Boucher, Y.; Jain, R.K.; Xu, L. TGF-β blockade improves the distribution and efficacy of therapeutics in breast carcinoma by normalizing the tumor stroma. *Proc. Natl. Acad. Sci. USA* **2012**, *109*, 16618–16623. [CrossRef] [PubMed]
154. Liao, S.; Liu, J.; Lin, P.; Shi, T.; Jain, R.K.; Xu, L. TGF-β Blockade Controls Ascites by Preventing Abnormalization of Lymphatic Vessels in Orthotopic Human Ovarian Carcinoma Models. *Clin. Cancer Res.* **2011**, *17*, 1415–1424. [CrossRef] [PubMed]
155. Steeg, P.S.; Camphausen, K.A.; Smith, Q.R. Brain metastases as preventive and therapeutic targets. *Nat. Rev. Cancer* **2011**, *11*, 352–363. [CrossRef] [PubMed]
156. Satcher, R.L.; Zhang, X.H.F. Evolving cancer–niche interactions and therapeutic targets during bone metastasis. *Nat. Rev. Cancer* **2022**, *22*, 85–101. [CrossRef]

157. Lajoie, J.M.; Shusta, E.V. Targeting Receptor-Mediated Transport for Delivery of Biologics Across the Blood-Brain Barrier. *Annu. Rev. Pharmacol. Toxicol.* **2015**, *55*, 613–631. [CrossRef]
158. Zhang, F.; Xu, C.L.; Liu, C.M. Drug delivery strategies to enhance the permeability of the blood-brain barrier for treatment of glioma. *Drug Des. Devel. Ther.* **2015**, *9*, 2089–2100. [CrossRef]
159. de Vries, N.A.; Zhao, J.; Kroon, E.; Buckle, T.; Beijnen, J.H.; van Tellingen, O. P-Glycoprotein and Breast Cancer Resistance Protein: Two Dominant Transporters Working Together in Limiting the Brain Penetration of Topotecan. *Clin. Cancer Res.* **2007**, *13*, 6440–6449. [CrossRef]
160. Szakács, G.; Paterson, J.K.; Ludwig, J.A.; Booth-Genthe, C.; Gottesman, M.M. Targeting multidrug resistance in cancer. *Nat. Rev. Drug Discov.* **2006**, *5*, 219–234. [CrossRef]
161. Kusuhara, H.; Sugiyama, Y. ATP-binding cassette, subfamily G (ABCG family). *Pflügers Arch. Eur. J. Physiol.* **2007**, *453*, 735–744. [CrossRef]
162. Lin, F.; de Gooijer, M.C.; Roig, E.M.; Buil, L.C.M.; Christner, S.M.; Beumer, J.H.; Würdinger, T.; Beijnen, J.H.; van Tellingen, O. ABCB1, ABCG2, and PTEN Determine the Response of Glioblastoma to Temozolomide and ABT-888 Therapy. *Clin. Cancer Res.* **2014**, *20*, 2703–2713. [CrossRef]
163. Kemper, E.M.; Boogerd, W.; Thuis, I.; Beijnen, J.H.; van Tellingen, O. Modulation of the blood–brain barrier in oncology: Therapeutic opportunities for the treatment of brain tumours? *Cancer Treat. Rev.* **2004**, *30*, 415–423. [CrossRef] [PubMed]
164. Arvanitis, C.D.; Askoxylakis, V.; Guo, Y.; Datta, M.; Kloepper, J.; Ferraro, G.B.; Bernabeu, M.O.; Fukumura, D.; McDannold, N.; Jain, R.K. Mechanisms of enhanced drug delivery in brain metastases with focused ultrasound-induced blood–tumor barrier disruption. *Proc. Natl. Acad. Sci. USA* **2018**, *115*, E8717–E8726. [CrossRef] [PubMed]
165. VanBavel, E. Effects of shear stress on endothelial cells: Possible relevance for ultrasound applications. *Prog. Biophys. Mol. Biol.* **2007**, *93*, 374–383. [CrossRef]
166. Jalali, S.; Huang, Y.; Dumont, D.J.; Hynynen, K. Focused ultrasound-mediated bbb disruption is associated with an increase in activation of AKT: Experimental study in rats. *BMC Neurol.* **2010**, *10*, 114. [CrossRef]
167. Liu, H.-L.; Huang, C.-Y.; Chen, J.-Y.; Wang, H.-Y.J.; Chen, P.-Y.; Wei, K.-C. Pharmacodynamic and Therapeutic Investigation of Focused Ultrasound-Induced Blood-Brain Barrier Opening for Enhanced Temozolomide Delivery in Glioma Treatment. *PLoS ONE* **2014**, *9*, e114311. [CrossRef] [PubMed]
168. Beccaria, K.; Canney, M.; Goldwirt, L.; Fernandez, C.; Piquet, J.; Perier, M.-C.; Lafon, C.; Chapelon, J.-Y.; Carpentier, A. Ultrasound-induced opening of the blood-brain barrier to enhance temozolomide and irinotecan delivery: An experimental study in rabbits. *J. Neurosurg. JNS* **2016**, *124*, 1602–1610. [CrossRef]
169. Chen, H.; Konofagou, E.E. The Size of Blood–Brain Barrier Opening Induced by Focused Ultrasound is Dictated by the Acoustic Pressure. *J. Cereb. Blood Flow Metab.* **2014**, *34*, 1197–1204. [CrossRef]
170. Patel, R.R.; Mehta, M.P. Targeted Therapy for Brain Metastases: Improving the Therapeutic Ratio. *Clin. Cancer Res.* **2007**, *13*, 1675–1683. [CrossRef]
171. Sloan, A.E.; Ahluwalia, M.S.; Valerio-Pascua, J.; Manjila, S.; Torchia, M.G.; Jones, S.E.; Sunshine, J.L.; Phillips, M.; Griswold, M.A.; Clampitt, M.; et al. Results of the NeuroBlate System first-in-humans Phase I clinical trial for recurrent glioblastoma: Clinical article. *J. Neurosurg. JNS* **2013**, *118*, 1202–1219. [CrossRef]